

Study of the effect of condensation and evaporation of water on heat and mass transfer in CO₂ absorption column

Koteswara Rao Putta, Hallvard Svendsen, Hanna K. Knuutila*

Department of Chemical Engineering, Norwegian University of Science and Technology, Sem Sælands vei 4, N-7491 Trondheim, Norway

* Corresponding author: hanna.knuutila@ntnu.no

Abstract

A rate-based combined heat and mass transfer model developed based on penetration theory is used to study the effect of water evaporation and condensation on the CO₂ absorption process using six different cases with real pilot-scale plants flue gas conditions. The effect of water evaporation and condensation on the concentrations, temperature profiles and reaction rates are studied in detail. The model predicted reasonable profiles as one would expect for water condensation and evaporation. The degree of liquid temperature rise depends mainly on the gas water saturation level and the temperature difference between the gas and liquid. Temperature profiles are flat in the liquid, whereas the transferring components create steep concentration gradients close to the interface making the interface concentrations change rapidly with position in absorber. This is in line with the thermal and mass diffusivities. Concentration build-up or depletion of species takes place in the liquid phase close to the gas-liquid interface up to 10 μm distance from the interface. For the case with absorber bottom pinch conditions, it was found that the CO₂ flux sign changes and desorption occurred when taking the evaporation and condensation effects into account, whereas, without these effects, only absorption was predicted. For most of the cases, absorption rate of CO₂ was not affected significantly even though concentration gradients and temperature changes were found. However, for the extreme case of warm unsaturated exhaust from an NG fired plant, case C1, and for the near pinch situation, case C6, significant changes to the CO₂ absorption rates were found.

Keywords: Combined heat and mass transfer, CO₂ absorption, H₂O evaporation, condensation, exothermic reactions, latent heat contributions

1 Introduction

In post-combustion CO₂ capture, the most appropriate and the only process ready for large-scale application for power plants is CO₂ absorption using amines. Monoethanolamine (MEA) is the solvent most often used as a reference in comparative studies to develop more energy efficient absorbents for post-combustion CO₂ capture (Liang et al., 2015, 2016; Luo et al., 2009; Puxty et al., 2010; Wang et al., 2011). In general, the process is costly and relatively energy intensive and work is ongoing around the world to make it economically and energetically more attractive for industrial implementation. This requires detailed understanding of the complex phenomena that involve the coupling between thermodynamics and diffusional processes in the gas and liquid phases in addition to complex chemical reactions occurring in the liquid close to the interface in the absorber and stripper (Tobiesen et al., 2007, 2008).

The absorber column in which CO₂ is absorbed from flue gas, is operated in a counter-current mode with a lean solvent containing small amounts of CO₂ fed at the top of the column and CO₂ rich flue gas fed at the bottom (Kohl and Nielsen, 1997; Rochelle, 2009). As the CO₂ is absorbed in the solvent, the temperature of the solvent will increase due to the exothermic nature of the absorption reaction, and water evaporation occurs due to the temperature increase. The temperature of the liquid decreases during the evaporation process as the energy required for the phase change from liquid to vapor is drawn from the liquid phase. In an absorber or desorber column, when evaporation of water occurs, the concentration of the solvent increases and the volume of the liquid phase decreases. The rate of evaporation varies from solvent to solvent as the heat of reaction varies. The amount of CO₂ absorbed into the solvent also influences the rate of evaporation of water from the solvent. Due to water evaporation and the latent heat associated with it, the flue gas temperature increases as it moves upward in the column and the water vapor pressure in the flue gas increases (Chow and Chung, 1983; Seaward et al., 1984). Towards the top of the column, the entering colder solvent will cause water condensation. Evaporation and condensation phenomena at the gas-liquid interface influence the heat and mass transfer fluxes. The temperature profiles are also affected and this will influence the physicochemical properties of the phases and the absorption of CO₂ into the liquid.

The effect of several parameters on the temperature bulge has been simulated using gPROMS and RateSep by Kvamsdal and Rochelle (Kvamsdal and Rochelle, 2008) using the pseudo-first order reaction assumption based on two-film theory. Sensitivity analyses of several process variables on CO₂ absorption have been performed recently (Kvamsdal and Hillestad, 2012; Ralph H. Weiland and Nathan A. Hatcher, 2011; Kale et al., 2013; Razi et al., 2013a, 2014). Neveux et al. (Neveux et al., 2013) studied the contribution of water flux to the total heat transfer flux to the liquid in both absorber and stripper. The liquid solvent flow rate has a significant effect on the temperature profile and in

turn on the absorber performance. They used an enhancement factor model in the rate-based model for the study, which is an approximate method.

In the literature, the H₂O concentration is normally assumed constant in reaction kinetics and heat and mass transfer studies. In the present work, we focus on the influence of water condensation and evaporation on CO₂ absorption using a discretized penetration theory-based model. The model accounts for variations in the water concentration in the solvent and in the solvent concentration (molarity) due to condensation and evaporation. The present work is performed using case studies with different operating conditions for the CO₂ absorber column.

2 Mathematical model

A combined rate based heat and mass transfer model to study the influence of water condensation and evaporation on the reaction rates and heat and mass transfer in the absorber column is derived below. The governing species material and energy balance equations including mass transfer, and the coupled chemical reaction system including volume change yield the following set of equations (1) - (12) in the discretized domain in case of CO₂ absorption into an aqueous MEA solution:

$$\frac{\partial n}{\partial t} = \left(D_{AB} \frac{\partial^2 C}{\partial x^2} \pm r \right) V \quad \text{where } n=C*V \quad (1)$$

$$\frac{\partial n}{\partial t} = \frac{\partial(C*V)}{\partial t} = V \frac{\partial C}{\partial t} + C \frac{\partial V}{\partial t} = \left(D_{AB} \frac{\partial^2 C}{\partial x^2} \pm r \right) V \quad (2)$$

Re-arranging eq. (1) gives

$$\frac{\partial C}{\partial t} = \left(D_{AB} \frac{\partial^2 C}{\partial x^2} \pm r \right) - \frac{C}{V} \frac{\partial V}{\partial t} \quad (3)$$

For differential element of radius r and thickness ‘ dr ’ and length L ,

$$\frac{C}{V} \frac{\partial V}{\partial t} = \frac{C}{\pi r^2 L} * \frac{2\pi r L \partial r}{\partial t} = \frac{2C}{r} \frac{\partial r}{\partial t} \quad (4)$$

The rate of change of liquid layer thickness w.r.t time can be given as

$$\frac{dr}{dt} (m.s^{-1}) = \frac{N_{tot}}{\rho_{sol}} = \frac{N_{MEA} * MW_{MEA} + N_{CO_2} * MW_{CO_2} + N_{H_2O} * MW_{H_2O}}{\rho_{sol}} \frac{(kg.m^{-2}.s^{-1})}{(kg.m^{-3})} \quad (5)$$

Substituting eq. (5) into eq. (3),

$$\frac{\partial C}{\partial t} = \left(D_{AB} \frac{\partial^2 C}{\partial x^2} \pm r \right) - \frac{2C}{r} \left(\frac{N_{MEA} * MW_{MEA} + N_{CO_2} * MW_{CO_2} + N_{H_2O} * MW_{H_2O}}{\rho_{sol}} \right) \quad (6)$$

After incorporating the volume change due to evaporation and condensation, the governing equations for CO₂ absorption into aqueous MEA solution can be given as:

$$\begin{aligned}
\frac{\partial [CO_2]}{\partial t} &= \left(D_{CO_2}^{Solution} \frac{\partial^2 [CO_2]}{\partial x^2} - r_{CO_2_MEA} - r_{CO_2_H_2O} - r_{CO_2_OH^-} \right) - \left(\frac{2C}{r} \frac{\partial r}{\partial t} \right) \\
\frac{\partial [MEA]}{\partial t} &= \left(D_{MEA} \frac{\partial^2 [MEA]}{\partial x^2} - 2 r_{CO_2_MEA} - r_{CO_2_H_2O} \right) - \left(\frac{2C}{r} \frac{\partial r}{\partial t} \right) \\
\frac{\partial [MEA H^+]}{\partial t} &= \left(D_{MEA H^+} \frac{\partial^2 [MEA H^+]}{\partial x^2} + r_{CO_2_MEA} \right) - \left(\frac{2C}{r} \frac{\partial r}{\partial t} \right) \\
\frac{\partial [MEACOO^-]}{\partial t} &= \left(D_{MEACOO^-} \frac{\partial^2 [MEACOO^-]}{\partial x^2} + r_{CO_2_MEA} + r_{CO_2_H_2O} \right) - \left(\frac{2C}{r} \frac{\partial r}{\partial t} \right) \\
\frac{\partial [H_2O]}{\partial t} &= D_{H_2O} \frac{\partial^2 [H_2O]}{\partial x^2} - \left(\frac{2C}{r} \frac{\partial r}{\partial t} \right) \\
\frac{\partial [H_3O^+]}{\partial t} &= D_{H_3O^+} \frac{\partial^2 [H_3O^+]}{\partial x^2} - r_{CO_2_H_2O} - \left(\frac{2C}{r} \frac{\partial r}{\partial t} \right) \\
\frac{\partial [HCO_3^-]}{\partial t} &= \left(D_{HCO_3^-} \frac{\partial^2 [HCO_3^-]}{\partial x^2} + r_{CO_2_OH^-} \right) - \left(\frac{2C}{r} \frac{\partial r}{\partial t} \right) \\
\frac{\partial [OH^-]}{\partial t} &= \left(D_{OH^-} \frac{\partial^2 [OH^-]}{\partial x^2} - r_{CO_2_OH^-} \right) - \left(\frac{2C}{r} \frac{\partial r}{\partial t} \right) \\
\frac{\partial [CO_3^{2-}]}{\partial t} &= \left(D_{HCO_3^-} \frac{\partial^2 [CO_3^{2-}]}{\partial x^2} \right) - \left(\frac{2C}{r} \frac{\partial r}{\partial t} \right)
\end{aligned} \tag{I}$$

$$\frac{\partial T}{\partial t} = \left(\alpha \frac{\partial^2 T}{\partial x^2} + \left(\frac{\Delta H_{rxn}}{\rho_{Solution} C_{P_{Solution}}} \right) (r_{CO_2_MEA} + r_{CO_2_H_2O}) \right)$$

Where the reaction rates $r_{CO_2_MEA}$, $r_{CO_2_H_2O}$, $r_{CO_2_OH^-}$ are given as below according to the direct (ter-molecular) reaction mechanism (Putta et al., 2016)

$$r_{CO_2_MEA} = k_{MEA}^T g_{MEA}^2 [MEA]^2 g_{CO_2} [CO_2] \frac{\frac{\alpha}{K_{eq_CO_2_MEA}} k_{MEA}^T \frac{\partial}{\partial T}}{K_{eq_CO_2_MEA}^T} \frac{\partial}{\partial T} \frac{MEAH^+}{MEACOO^-} \tag{7}$$

$$r_{CO_2_H_2O} = k_{H_2O}^T g_{H_2O} [H_2O] g_{MEA} [MEA] g_{CO_2} [CO_2] \frac{\frac{\alpha}{K_{eq_CO_2_H_2O}} k_{H_2O}^T \frac{\partial}{\partial T}}{K_{eq_CO_2_H_2O}^T} \frac{\partial}{\partial T} \frac{H_3O^+}{MEACOO^-} \tag{8}$$

$$r_{CO_2_OH^-} = k_{CO_2_OH^-}^T [CO_2] [OH^-] \frac{\frac{\alpha}{K_{eq_CO_2_OH^-}} k_{CO_2_OH^-}^T \frac{\partial}{\partial T}}{K_{eq_CO_2_OH^-}^T} \frac{\partial}{\partial T} \frac{HCO_3^-}{HCO_3^-} \tag{9}$$

Kinetic constants are taken from Putta et al. (2016).

Model equations given in (I) for the combined heat and mass transfer model are solved using orthogonal collocation on finite elements by applying the initial and boundary conditions given in equations (10) - (17).

One initial condition and two boundary conditions are necessary for each equation.

Initial condition: Uniform profiles are assumed for all species and the temperature in the liquid phase calculation domain before gas and liquid come into contact.

At time $t = 0$ and $x \geq 0$

$$[C_i] = [C_i]_0 \text{ where } C_i = CO_2, MEA, MEAH^+, MEACOO^-, H_2O, H_3O^+, HCO_3^-, OH^-, CO_3^{2-} \text{ and } T \quad (10)$$

As in Putta et al. (2016) an e-NRTL model is used for obtaining equilibrium concentrations used in equation (10).

Boundary condition in the liquid bulk: At all times, the concentration gradients of all components is assumed zero in the liquid bulk,

At time $t > 0$ and $x = \infty$ (liquid bulk)

$$\frac{\partial [C_i]}{\partial x} = 0 \text{ where } C_i = CO_2, MEA, MEAH^+, MEACOO^-, H_2O, H_3O^+, HCO_3^-, OH^-, CO_3^{2-} \text{ and } T \quad (11)$$

Boundary condition at the gas-liquid interface: All the ionic species are assumed non-volatile and only the transfer MEA, CO_2 , and H_2O , is accounted for between the gas and liquid phases through the gas-liquid interface.

For all the non-volatile species, at time $t > 0$ and $x = 0$ (gas-liquid interface)

$$\frac{\partial [MEACOO^-]}{\partial x} = \frac{\partial [MEAH^+]}{\partial x} = \frac{\partial [H_3O^+]}{\partial x} = \frac{\partial [HCO_3^-]}{\partial x} = \frac{\partial [OH^-]}{\partial x} = \frac{\partial [CO_3^{2-}]}{\partial x} = 0 \quad (12)$$

For the transferring components between the phases, the mass transfer rate in the gas phase is assumed equal to the mass transfer rate in the liquid phase at the interface, i.e.:

$t > 0, \quad x = 0,$

$$k_g (P_{CO_2, g, bulk} - P_{CO_2, g, i}) = -D_{CO_2}^{Solution} \frac{\partial [CO_2]}{\partial x} \Big|_{x=0} \quad (13)$$

$$k_{gw} (P_{H_2O, g, bulk} - P_{H_2O, g, i}) = -D_{H_2O} \frac{\partial [H_2O]}{\partial x} \Big|_{x=0} \quad (14)$$

$$k_{gm} (P_{MEA, g, bulk} - P_{MEA, g, i}) = -D_{MEA}^{Solution} \frac{\partial [MEA]}{\partial x} \Big|_{x=0} \quad (15)$$

Concentrations are used for the calculation of diffusive fluxes in the liquid phase, as the diffusivities are available only on concentration basis.

The concentrations of CO_2 in liquid and gas at the interface are correlated using Henry's law as below:

$$H_{CO_2}^{Solution} = \frac{P_{CO_2, g, i}}{[CO_2]_{l, i}} = \gamma_{CO_2} H_{CO_2-H_2O}^\infty \quad (16)$$

For temperature, the boundary condition can be specified as:

$$\lambda \left. \frac{\partial T}{\partial x} \right|_{x=0} = h(T|_{x=0} - T_g) + MW_{CO_2} C_{p,CO_2} (T|_{x=0} - T_g) N_{CO_2} + h_{H_2O}^{vap} N_{H_2O} + h_{MEA}^{vap} N_{MEA} \quad (17)$$

The temperature boundary condition at the gas-liquid interface includes the latent heat contributions of water and MEA at the liquid surface due to evaporation or condensation, CO₂ latent heat transfer, and the sensible heat transfer into the liquid. The latent heat term, H_{latent} used in the plots in the following sections, is the sum of the last three terms in equation (17). Both CO₂ latent heat and MEA evaporation latent heat are small compared to the latent heat transfer due to evaporation of water. MEA evaporation counts for less than 1% of the total latent heat transfer and CO₂ latent heat due to transfer from gas to liquid is less than 5% (maximum 5% in case C2) of the total latent heat transfer. All the latent heat terms due to CO₂ transfer from gas to liquid, MEA evaporation and water evaporation or condensation are included in the H_{latent} term as used in plots in the following sections.

Parameters used in the model:

For the combined heat and mass transfer study, several physical and chemical properties are required in the model. The viscosity of pure water and MEA and heat capacities of water, pure MEA and aqueous MEA solutions are calculated using the correlation by Cheng et al., (1996). Diffusivity of CO₂ in water is calculated using the correlation given by Versteeg and Van Swaaij (1988) and in aqueous MEA solution using the Ko et al. (2000) correlation based on the N₂O analogy. The diffusivity of MEA is calculated based on the Snijder et al. (1993) correlation. Gas phase diffusivities of CO₂ and H₂O are calculated using the Reid et al. (1986) expression. Calculation of densities of water, pure MEA and loaded aqueous MEA solution as well as viscosity of loaded MEA solutions are estimated using correlations given by Hartono et al. (2014). The e-NRTL model fitted using physical solubilities of CO₂ reported by Hartono et al. (2014) was used for the estimation of Henry's law constant of CO₂ in loaded MEA solutions (Putta et al., 2016). Experimental data for the diffusivities of ions are still lacking in the literature. Therefore, diffusivities of MEAH⁺ and MEACOO⁻ are assumed to be equal to the diffusivity of MEA in aqueous MEA solution. Heat transfer coefficients are calculated using the Chilton-Colburn analogy (Geankoplis, 2003).

3 Numerical solution method

The orthogonal collocation on finite elements (OCFE) method used is the same as in Putta et al. (2016) and more details can be found there. The model equations were implemented in the MATLAB

software. In this orthogonal collocation on finite elements (OCFE) method, the first collocation point of the first element is the boundary condition at the gas-liquid interface and the last collocation point in the last element is the boundary condition in the liquid bulk (Arora et al., 2006a, 2006b; Carey and Finlayson, 1975; Duarte and Portugal, 1995; Ghanaei and Rahimpour, 2010). For all other elements, at the boundary between two elements, the condition of continuity of variable is used. I.e., the last collocation point of the k^{th} element is the same as the first collocation point of the $(k+1)^{\text{th}}$ element.

$$[C_i]_{\text{end point}}^{k^{\text{th}} \text{ element}} = [C_i]_{\text{first point}}^{(k+1)^{\text{th}} \text{ element}} \quad (18)$$

$$\left[\frac{dC_i}{dx} \right]_{\text{end point}}^{k^{\text{th}} \text{ element}} = \left[\frac{dC_i}{dx} \right]_{\text{first point}}^{(k+1)^{\text{th}} \text{ element}} \quad (19)$$

Where $i = \text{CO}_2, \text{MEA}, \text{MEA}^{\text{H}^+}, \text{MEACOO}^-, \text{H}_2\text{O}, \text{H}_3\text{O}^+, \text{HCO}_3^-, \text{OH}^-, \text{CO}_3^{2-}$ and T

4 Results and discussion

The study is divided into 6 different case studies. The conditions used in the case studies are given in table 1. Out of the 6 cases considered in this study, 3 cases study the absorber bottom in processes for flue gas from respectively a gas-fired power plant (Razi et al., 2013b), a coal-fired power plant (Razi et al., 2013b) and a cement plant (Hassan, 2005). Two cases are considered for the lean end top-section of the absorber column, one for the NGCC case (Razi et al., 2013b).and another one for the cement plant case (Hassan, 2005). The last studied case investigates the absorber bottom pinch. The main focus is to study the effect of different gas and liquid phase conditions on the heat and mass transfer in the different sections of the absorber column.

Case 1: Gas-fired power plant (430 MWe) flue gas composition (NGCC)

Case 2: Coal-fired power plant (800 MW) flue gas composition

Case 3: Bottom section of the absorber column for cement case

Case 4: A point in the top section of the absorber column for Natural gas case

Case 5: Top section of the absorber column for cement case

Case 6: Absorber bottom pinch

Table 1. Gas and liquid phase conditions used in case studies

Case	T _g (°C)	T _l (°C)	Loading	P _{CO₂-b} (kPa)	P _{H₂O-b} (kPa)
C1	90	55	0.45	3.94	8.33
C2	50	43.5	0.47	13.73	9.88
C3	40	57	0.495	27.72	5.04
C4	38	39.6	0.3	0.94	14.00
C5	56.4	40	0.3	4.80	14.64
C6	40	40	0.475	3.00	14.00

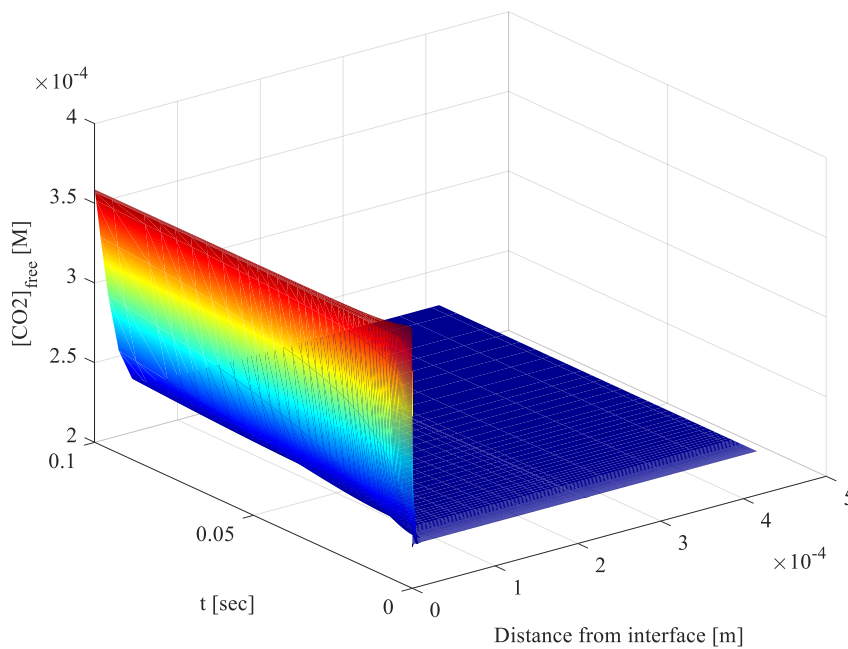
4.1 Effect of flue gas from 3 different sources on the absorber bottom section (cases 1-3)

Flue gas from three different sources, namely a natural gas-fired power plant (NGCC), a coal-fired power plant and a cement plant are used to study the effect of flue gas composition at the rich end of the absorber column i.e. the bottom section of the absorber. Temperature, partial pressures of CO₂ and H₂O are different for flue gas from each source and are given in table 1 above.

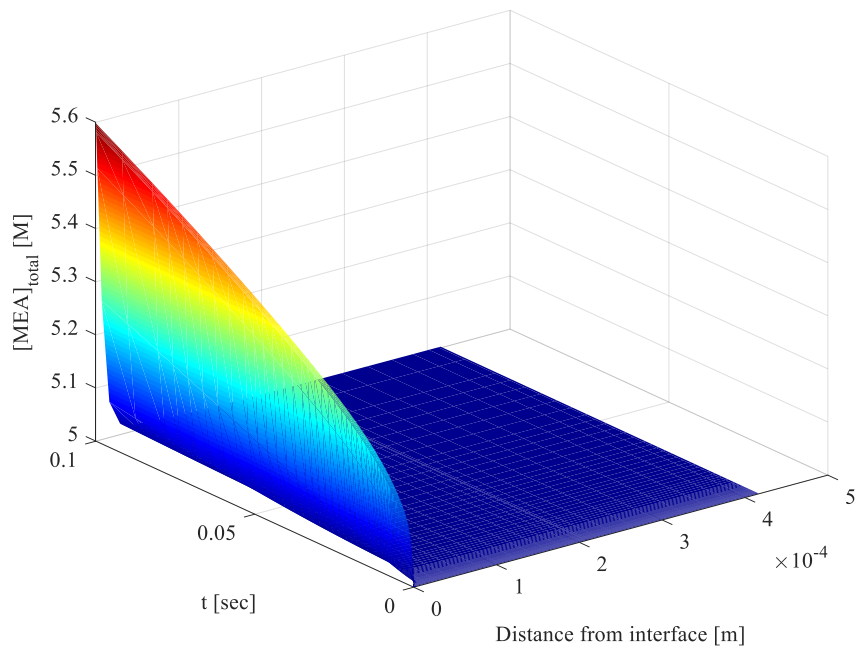
The contact time of 0.1 sec has been used for all the cases to study what happens during condensation and evaporation over a 20 cm segment in the absorber column, thus assuming a gas velocity of 2 m/s.

Natural gas-fired power plant (NGCC) flue gas case (C1):

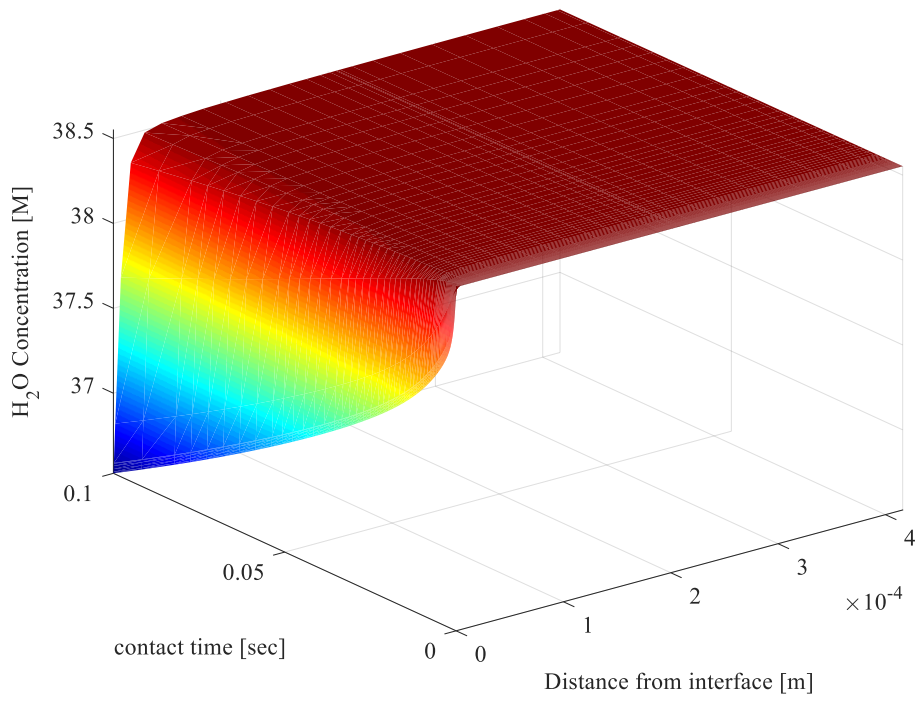
Fig. 1 shows the concentration and temperature profiles in the liquid film. The x-axis represents the distance from the gas-liquid interface in the liquid film (m), the y-axis represents the contact time (sec) between the gas and liquid and z-axis represents the molar concentrations of species ([M]) or temperature (T).



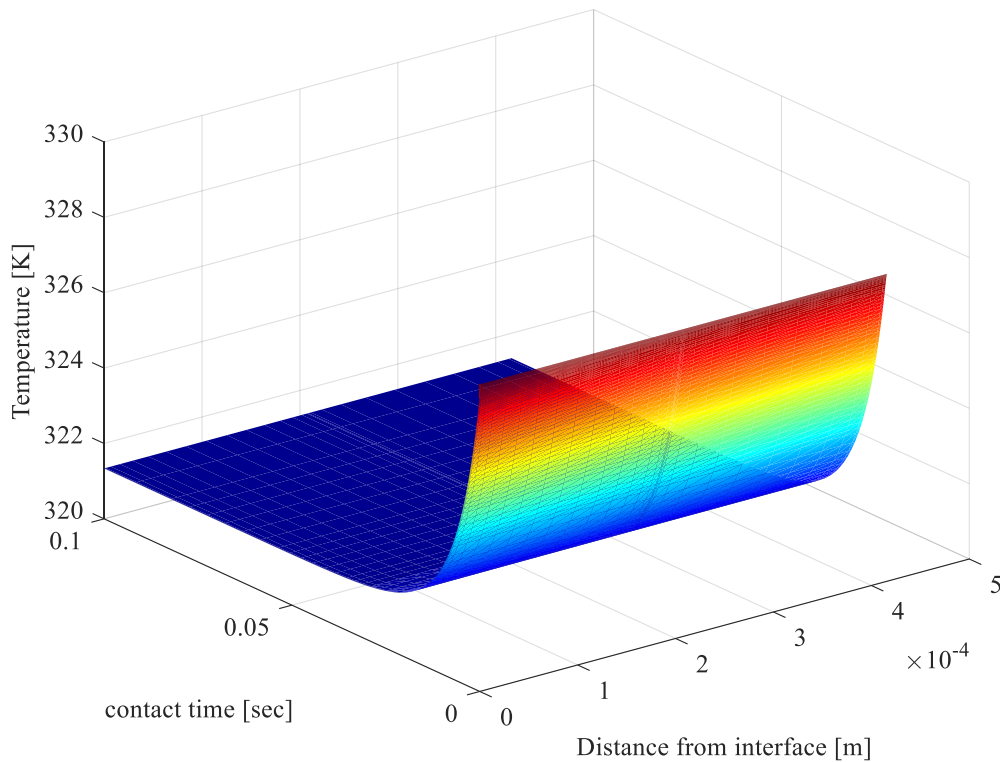
(a)



(b)



(c)



(d)

Fig.1 (a) Free CO₂ (b) total MEA (c) H₂O and (d) Temperature profiles in the liquid film for NGCC case

In the NGCC case, flue gas enters at 90°C at the bottom of the absorber and meets solvent at 55 °C. The entering flue gas is far from saturated in water and as it comes in contact with the solvent, immediately solvent starts evaporating. Mainly water in the solvent evaporates and due to evaporation both water concentration and solvent temperature decreases. The water concentration decreases and the total MEA concentration in the solvent increases with time at the interface as can be seen in fig. 1 above. The accumulation or depletion of these two components occurs very close to the gas-liquid interface and concentration profiles in the liquid film are flat after a 10 μm distance from the interface (1/40th of liquid film thickness) whereas the temperature profile is uniform throughout the liquid film at any given time. This difference is reasonable as the thermal diffusivity of the solvent is 1000 times higher than the mass diffusivity, thus the thermal diffusion is fast compared to the mass transfer. This can be seen clearly from the zoomed profiles given in Appendix A1. The CO₂ concentration is constant at the interface and decreases rapidly when going into the film due to reaction with MEA. The reaction occurs very close to the gas-liquid interface and all the free CO₂ is reacted and the CO₂ concentration becomes very low only a few μm from the interface.

As can be seen from fig. 2(a), the temperature of the interface solvent decreases by almost 6°C due to evaporation. The temperature of the solvent drops quite fast in the liquid film as soon as the gas meets the liquid and after that, the liquid temperature remains constant even though evaporation of

water is still taking place as can be seen from the steadily reduced concentration of water in fig. (2b). This indicates that the sensible heat transfer and the evaporation even out each other. Because of this the temperature of the liquid becomes almost even though there still evaporation as seen in fig. 2(b). The constant level is very close to the wet bulb temperature of the gas, but slightly lower because of the simultaneous evaporation of water and MEA. Fig. 2(c) shows the heat transfer contributions due to convective heat transfer from gas to the liquid phase and latent heat due to evaporation of water with respect to time. From the fig. 2(c), it can be seen that after 0.02 seconds, both sensible heat transfer due to convection from gas to the liquid phase and latent evaporative heat transfer to the gas from liquid become almost equal. It should be noted that both the latent heat transfer due to CO₂ transfer from gas to liquid and MEA evaporation, even though their contributions are very small, are also included in the H_latent term (kW/m²) in fig. 2(c) and later similar figures.

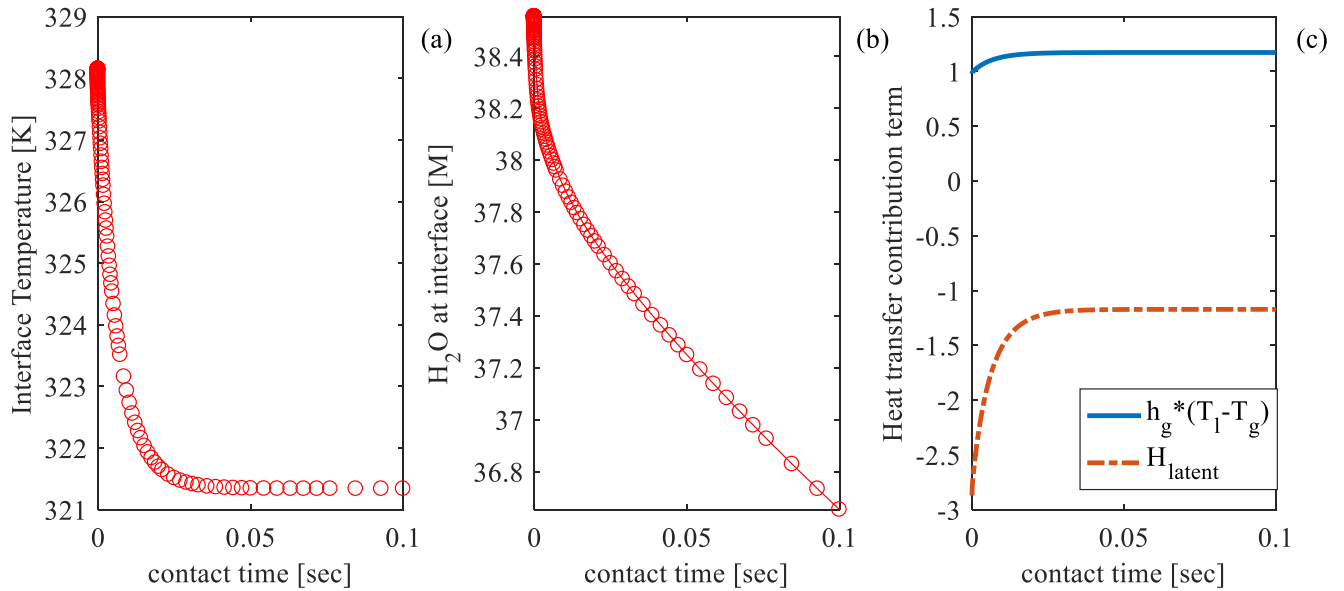


Fig.2 (a) Temperature, (b) H₂O concentration profiles and (c) Heat transfer contributions with respect to time at the interface

The concentration and temperature profiles of different species in the liquid film are shown in fig. 3 after 0.1 sec of contact time.

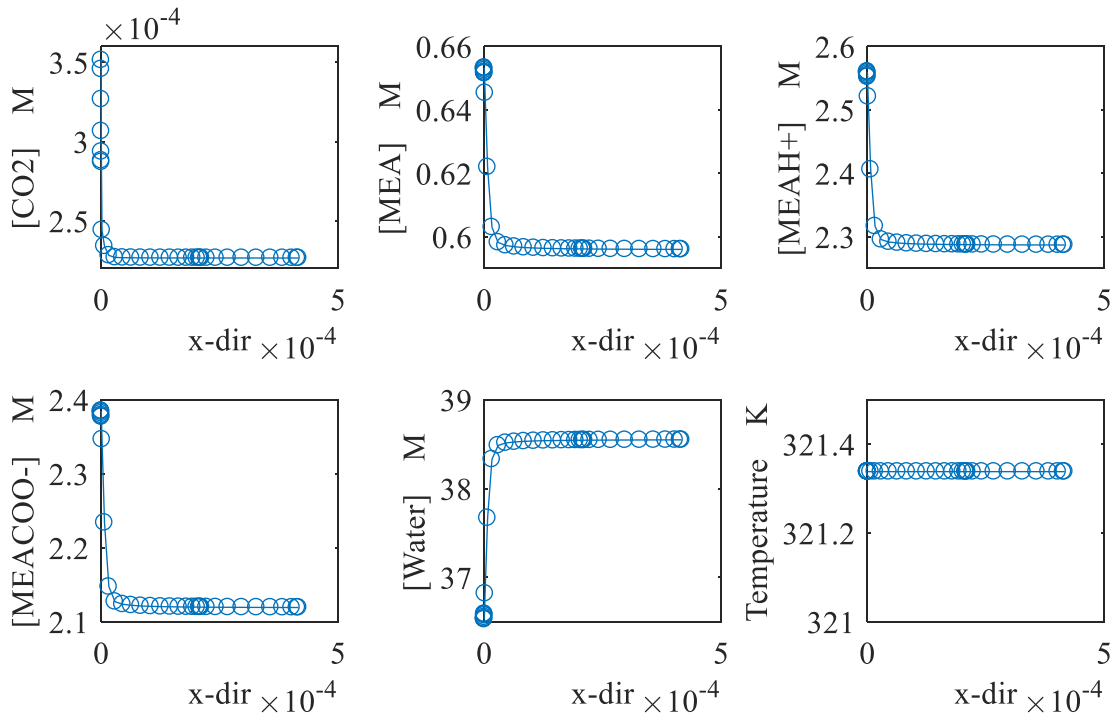
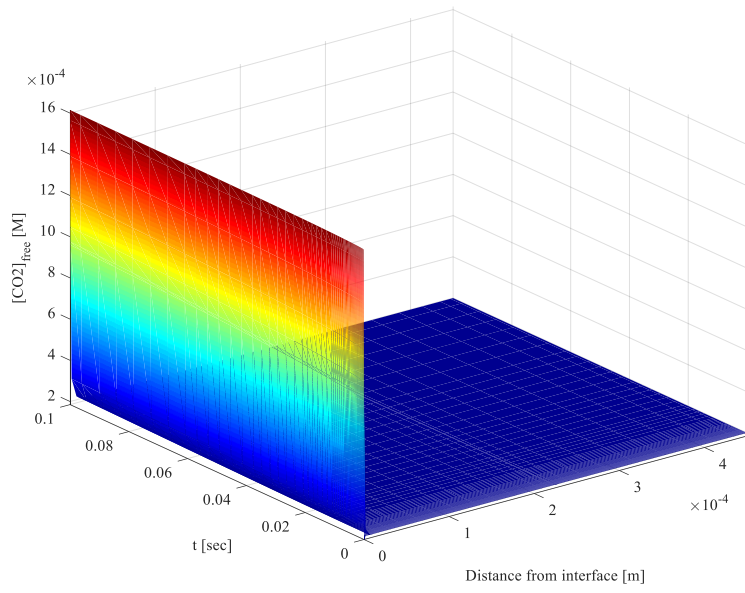


Fig.3 Concentration and temperature profiles in the liquid film at 0.1 sec for the NGCC case

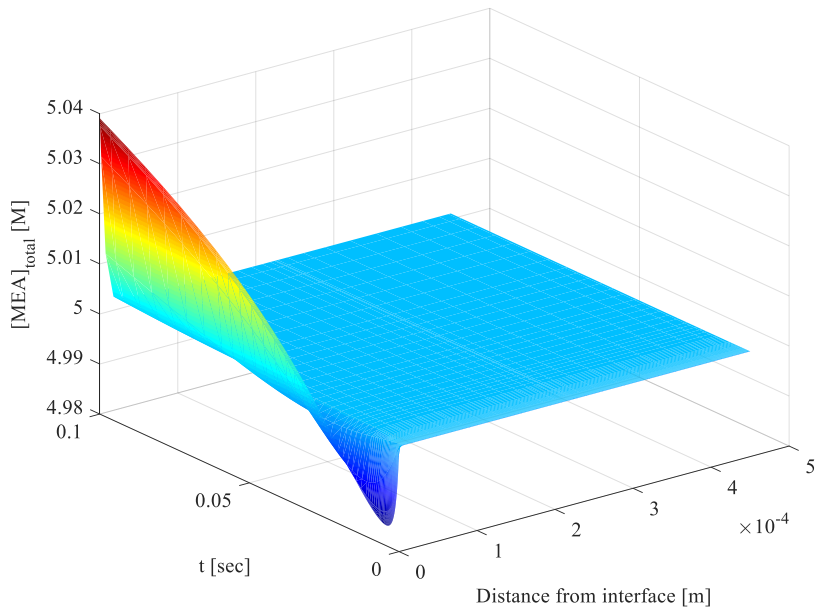
Concentrations of CO_2 , free MEA, MEA^+ , and MEACOO^- decrease as the one moves from the gas-liquid interface to the liquid bulk. It can be clearly seen that the concentrations vary only close to the interface and that the trends are opposite to the water profile. This is expected due to the inclusion of the volume correction factor in the model equations which will take into account the changes in concentrations due to evaporation and condensation. As the molar water concentration decreases, the molar concentrations of other species should increase and this is seen in the profiles. For the same case without the volume correction factor, all species profiles are the same except the free MEA which has the same trend as water because free MEA is depleted close to the interface due to reaction with free CO_2 .

Coal-fired power plant flue gas case (C2):

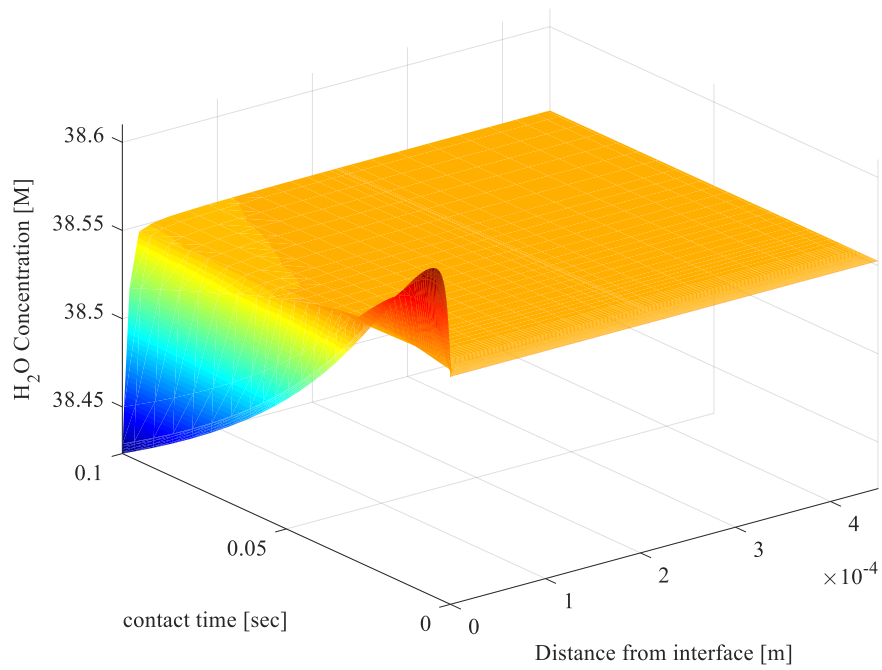
In this case, as seen from table 1, the difference between gas and liquid temperature at the absorber bottom is small compared to the NGCC case but the CO_2 concentration is higher than in case C1. Concentration and temperature profiles are shown in fig. 4. Fig. 5 shows interface temperature, water concentration, and heat transfer contributions w.r.t. contact time.



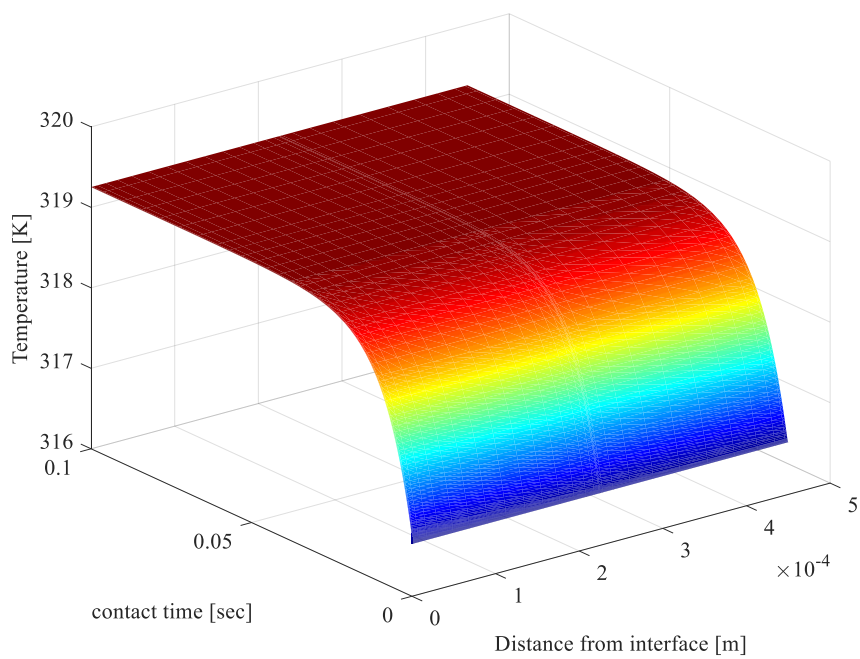
(a)



(b)



(c)



(d)

Fig.4 (a) Free CO₂ (b) total MEA (c) H₂O and (d) temperature profiles in the liquid film for case C2

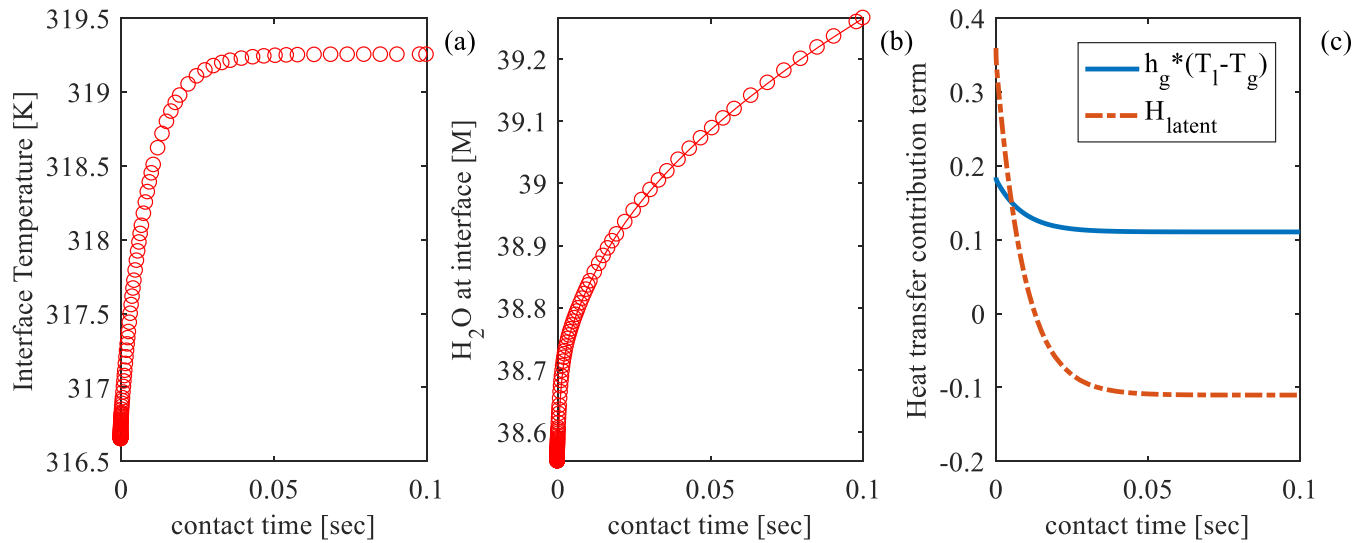
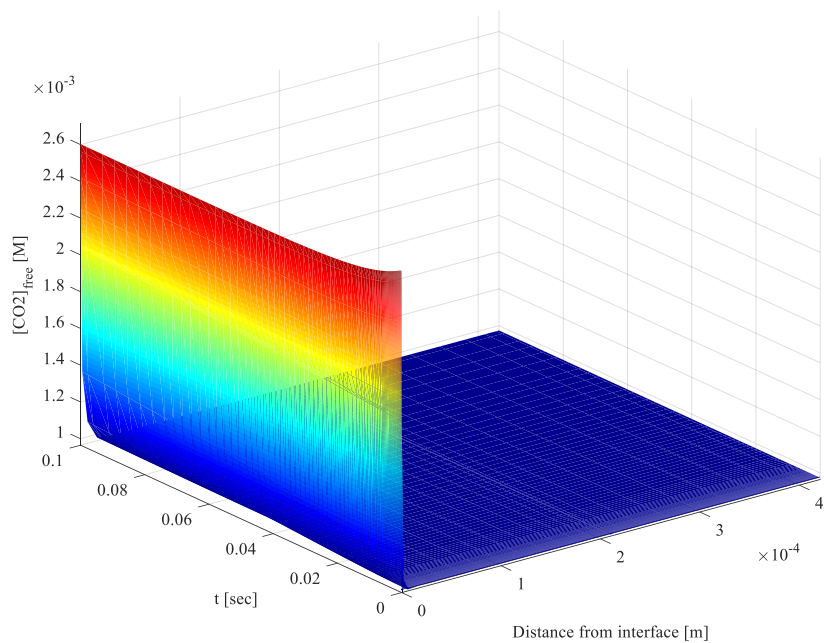


Fig.5 (a) Temperature, (b) H₂O concentration profiles and (c) Heat transfer contributions with respect to time at the interface for case C2.

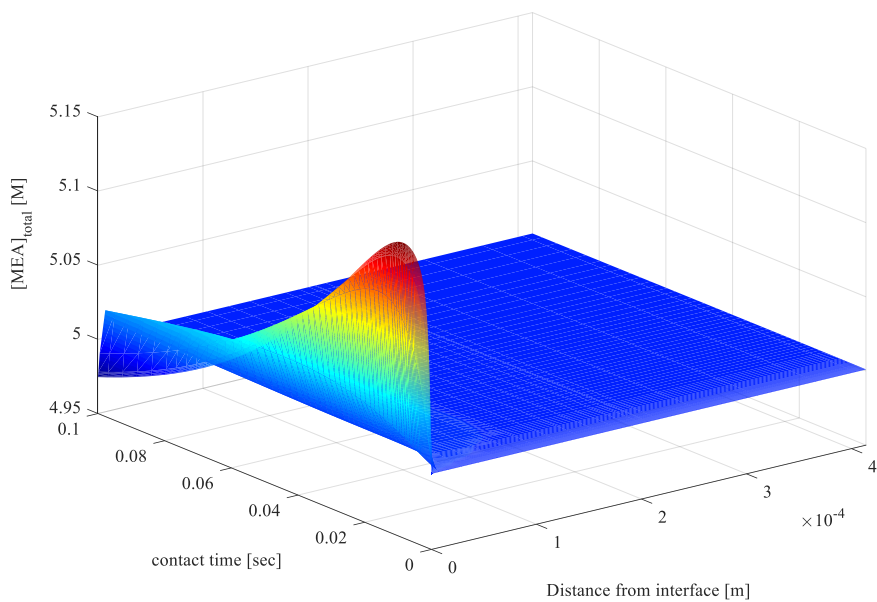
It is seen from fig. 4 and 5 that as soon as the gas and liquid comes in contact, due to the difference in partial pressure of H₂O in the flue gas and saturation pressure of the liquid solution, condensation of water occurs. Because of the condensation of water, the liquid temperature increases from 316.5 to 319 K rapidly within 0.03 seconds. The water concentration increases at the start and after a short while starts to decrease due to evaporation. The opposite behavior is seen in the total MEA concentration profile. With an increase in liquid temperature, the water saturation pressure increases above the gas phase water partial pressure, thereby causing evaporation of water. As the sensible heat transfer rate from gas to liquid and the latent heat transfer equilibrate, there is no change in the liquid temperature.

Cement plant flue gas case (C3):

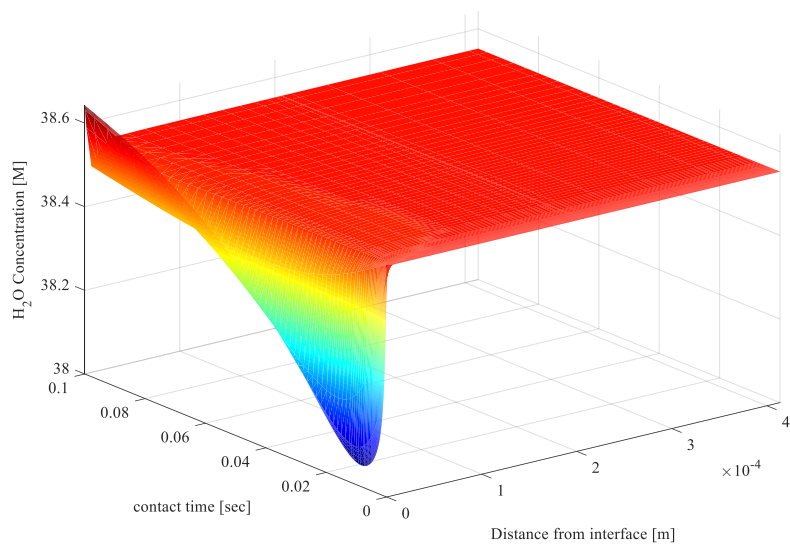
To simulate the heat and mass transfer effects due to water evaporation and/or condensation at the absorber bottom (case C3) for an industrial application, flue gas data were taken from St. Marys Cement plant (Hassan, 2005). The CO₂ concentration in the cement plant flue gas is very high (around 27 vol. %) compared to natural-gas fired and coal-fired power plant cases. The flue gas from the cement plant is around 160°C and is cooled down to 40°C before it enters the absorber column at the bottom. The solvent is hotter than the flue gas in this case and the conditions are given in table 1. The concentration and temperature profiles for the cement plant case C3 are shown in fig. 6.



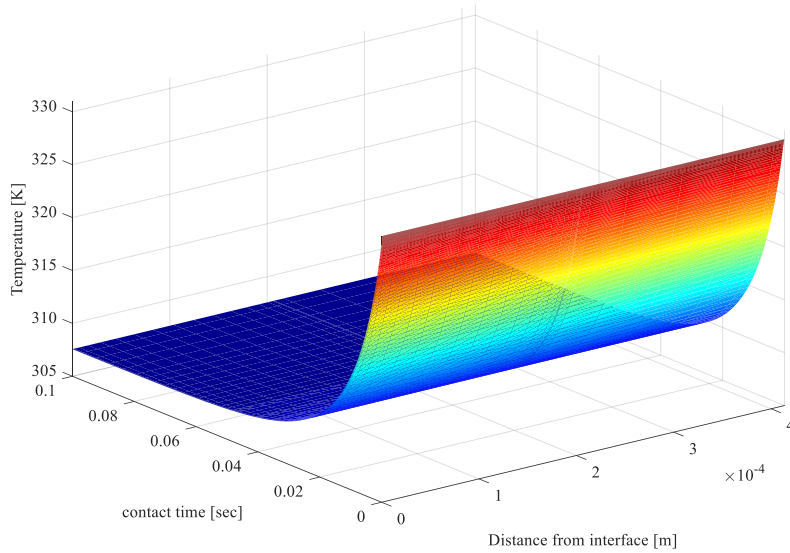
(a)



(b)



(c)



(d)

Fig.6 (a) Free CO₂ (b) total MEA (c) H₂O and (d) temperature profiles in the liquid film for cement plant case C3

It is observed from fig. 6 that evaporation of water occurs when the inlet gas is brought in contact with the liquid as the gas is unsaturated at the given liquid temperature. This leads to a rapid and significant liquid temperature drop from 330 K to below the gas temperature. Then, the driving force for water changes direction and condensation of water occurs. As can be clearly seen from the total MEA and H₂O profiles at the interface, when the H₂O concentration decreases during evaporation, the total MEA concentration rises and when condensation of H₂O starts the total MEA concentration starts decreasing. The resulting model predictions are reasonable and according to what one would expect at the absorber bottom. From fig. 7, it is clearly seen that at the interface the H₂O concentration drop is very steep initially, but after 0.015 sec of contact time, it starts to increase slowly due to condensation. Regarding sensible and latent heat transfer it is seen that both sensible and heat transfer due to evaporation drop rapidly and become close to constant after a very short time.

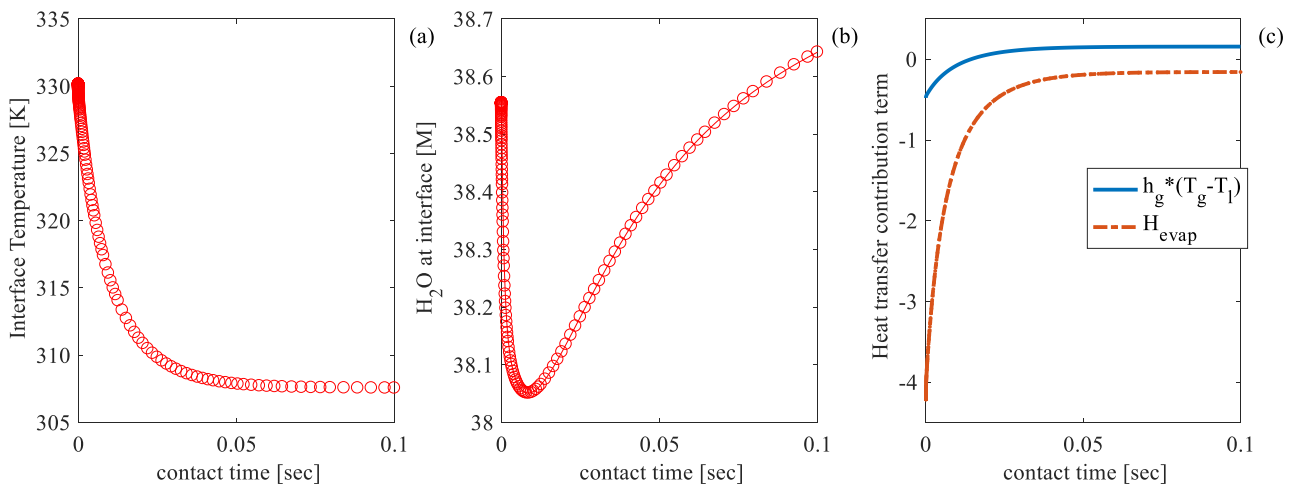


Fig.7 (a) Temperature, (b) H₂O concentration profiles and (c) Heat transfer contributions with respect to time at the interface for case C3.

When comparing the three cases it is seen that depending on the water saturation in the flue gas and the temperatures of gas and liquid, the initial concentration and temperature profiles in the liquid will be very different. In case C1, only evaporation occurs all the time. In case C2 condensation takes place initially for a short time period and then evaporation starts. In case C3 the trend is exactly opposite to the trend in case C2 i.e., first evaporation takes place and later condensation.

Reaction rates:

The CO₂ concentration in the flue gas and the solvent temperature and CO₂ loading are different in the cases C1, C2, and C3. Hence the reaction rates will also be different in the three cases. For any given case, reaction rates given by equations (7) and (8) also vary with position and time. The ratio

of reaction rates caused by water and MEA respectively, $\frac{r_{CO_2-H_2O}}{r_{CO_2-MEA}}$, at the absorber bottom is shown

in fig.. 8 for all three cases studied. Due to evaporation, both concentrations of species and liquid temperature varies and hence the reaction rates also vary. Changes in the reaction rate ratio indicate a relative change in reaction rates given by equations (7) and (8). As the CO₂ concentration profile is very steep and levels off very close to the interface in the liquid film, the reaction rate ratio profiles are shown in that region only. As seen from fig. (8), for any given case the degree of change is different for each reaction. For all the three cases C1, C2 and C3, the change in reaction rate given by equation (8) is higher than the change in reaction rate given by equation (7). For the NGCC case

C1, the ratio of reaction rates $\left(\frac{r_{CO_2-H_2O}}{r_{CO_2-MEA}} \right)$ increases rapidly up to 0.05 sec and then becomes almost

constant. In the case of cases C2 and C3, the ratio increases continuously throughout the whole contact time and the change in the reaction rate ratio is maximum for case C3. For case C2, the ratio is less than that of case C3 but still higher than that of case C1. Detailed reaction rate profiles with respect to time and position in the film are given in Appendix B. Due water evaporation, both temperature and water concentration decreases whereas the amine concentration increases. Due to the complex dependence of reaction rates on concentrations of MEA and H₂O and the temperature, the reaction rates $r_{CO_2-H_2O}$ and r_{CO_2-MEA} have different impact. From fig. s (a)-(c) given in Appendix B, it can be seen that the reaction rate $r_{CO_2-H_2O}$ is always higher than r_{CO_2-MEA} . As the degree of change in MEA and H₂O concentrations and temperature is different in the cases C1, C2 and C3, the change in reaction rates is different for all these three cases. As the temperature drop is highest in case C3, the same is reflected in the reaction rate profiles. The individual reaction rates and the ratio of the reaction

rates gives an idea about the impact of the combined heat and mass transfer on the chemical reaction rates. This reaction rate ratio gives information about the relative importance of the chemical reactions under different process operating conditions and helps the modelers understand the complex interaction of different parameters on the overall process performance.

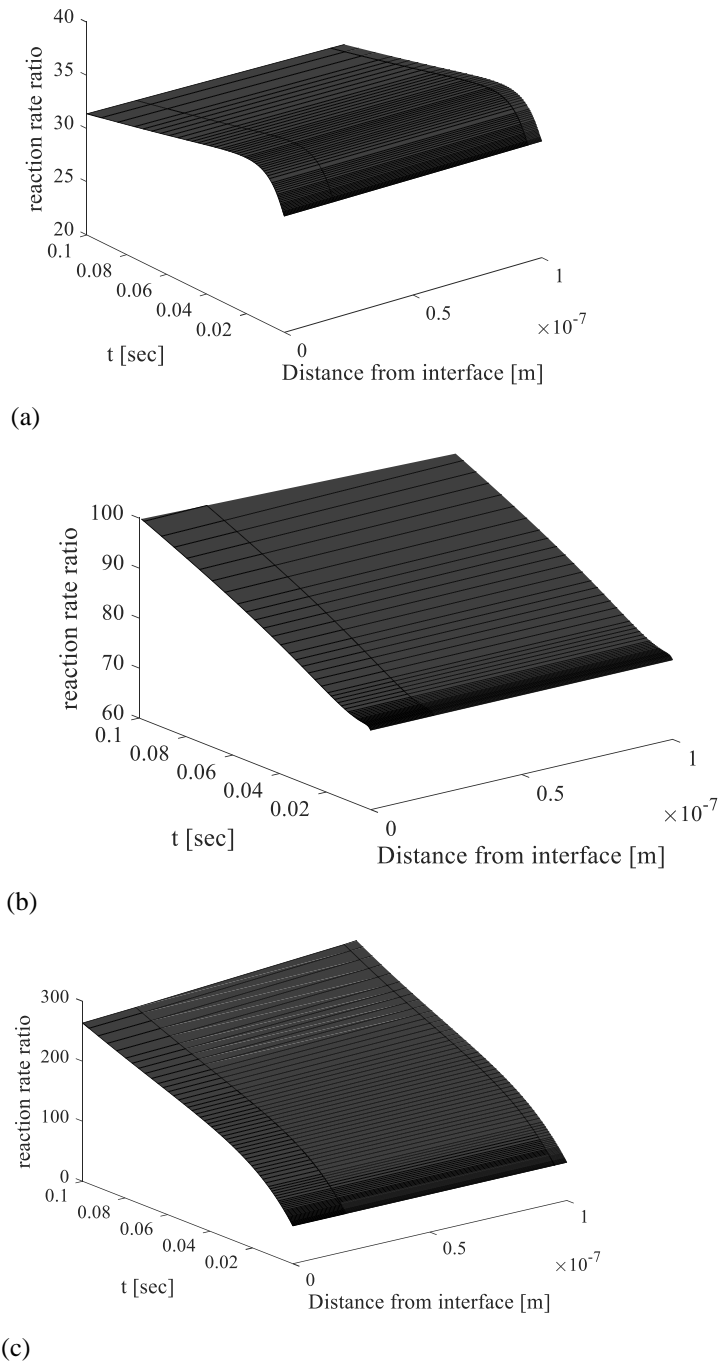


Fig.8 Reaction rate ratio profiles for (a) case C1, (b) case C2 and (c) case C3.

4.2 Heat and mass transfer effects in the absorber top section (cases 4 -5)

In the top section of the absorber, where the hot gas meets incoming cold and lean solution, the flue gas is super-saturated with H₂O and the CO₂ concentration is small compared to in the bottom

section. Two cases have been considered to study the effect of water condensation on the heat and mass transfer in the top section of the absorber. The contact time zero (0 sec) corresponds to the condition at lean solvent inlet and increase in contact time represents the conditions moving from top towards the bottom section of the absorber. Conditions taken in the Case 4 correspond to the NGCC case and case 5 corresponds to the cement plant case. The lean loading of the solution is constant in both cases. The conditions are given table 1.

NGCC case (case C4):

The concentration and temperature profiles are shown in fig. 9 below. Profiles at the interface are shown in fig. 10. It can be seen from fig. (9) and (11) that at the lean solvent inlet, condensation of water starts to happen and the water content increases. However, after about 0.015s the water concentration starts falling then again to increase after about 0.05sec.

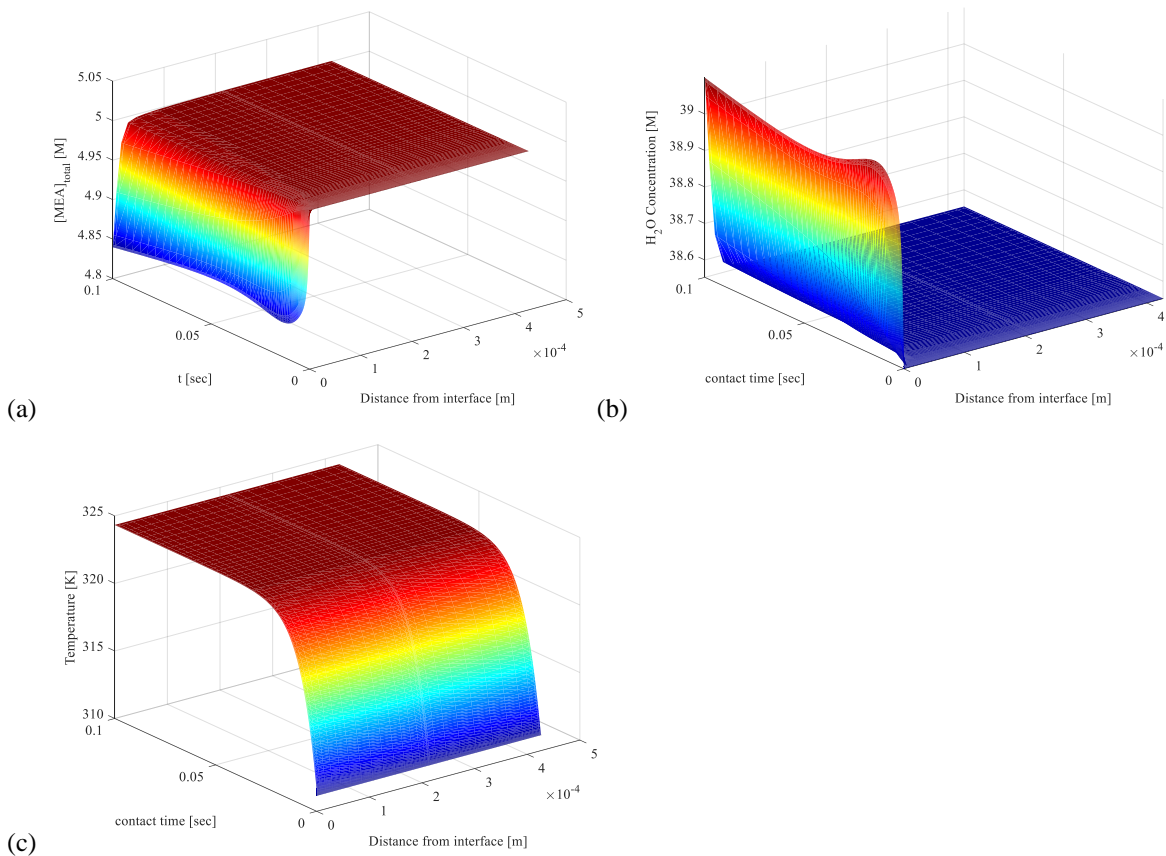


Fig.9 (a) Total MEA (b) H₂O and (c) temperature profiles in the liquid film for NGCC plant case C4 in the top section of the absorber

We believe the reason for this behaviour is the simultaneous transfer of water and CO₂ and the interaction between the interface and the inner parts of the liquid film. In Appendix a, the zoomed concentration profiles for water, total MEA and free MEA are given. The condensation of water is rapid and heat is released at the interface. In the model it enters into the boundary condition. The CO₂

transferred reacts and then releases heat inside the liquid. As explained now in the last paragraph of section 4, this contribution is small and is, for most cases, overshadowed by, in particular, water condensation and evaporation. However, in case C4, the temperatures are well matched so the dominance of water condensation is not so large. Thus, what happens is that first water condensates rapidly, releasing heat at the interface and increasing the temperature. Simultaneously CO₂ is absorbed, initially very rapidly as seen from Figure 10, but releases heat more slowly inside the liquid. The CO₂-caused heat release close to the interface creates a more rapid rise in interface temperature, compared to what would have been the case if only water had condensed, and the water condensation rate is slowed down more rapidly than would have been the case without CO₂ reacting. At the same time liquid internal gradients are built up and water transfers to the inner parts of the liquid and MEA in all forms is transferred toward the interface. Because of the lowering of the condensation rate, water will actually be removed from the interface and temporarily its concentration falls, and the total MEA concentration increases. Further out in time, the CO₂ absorption rate decreases and loses its effect on the water transport, and the water condensation rate becomes larger than the removal rate to the liquid interior again. In the other cases, this effect is also there but is not visible because of the dominance of water condensation/evaporation.

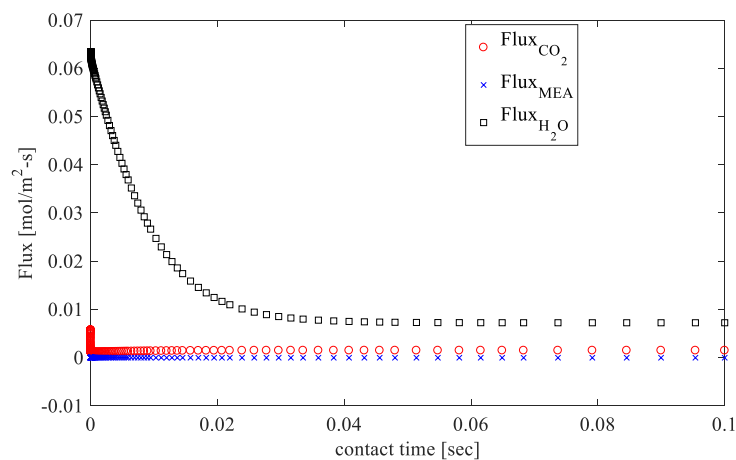


Fig.10 Flux profiles for water, CO₂ and MEA for the interface NGCC plant case C4 in the top section of the absorber

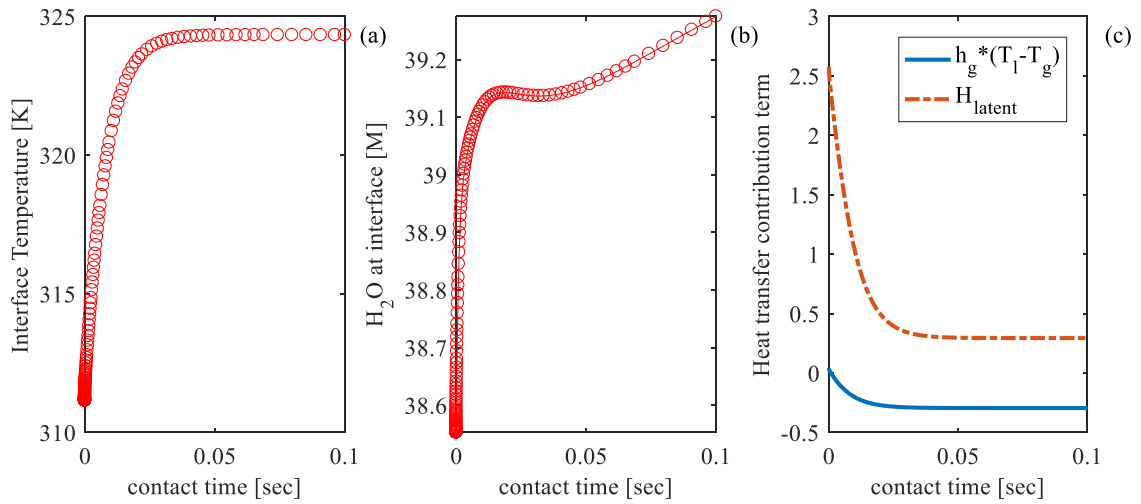


Fig.11 (a) Temperature, (b) H₂O concentration profiles and (c) Heat transfer contributions with respect to time at the interface NGCC plant case C4 in the top section of the absorber.

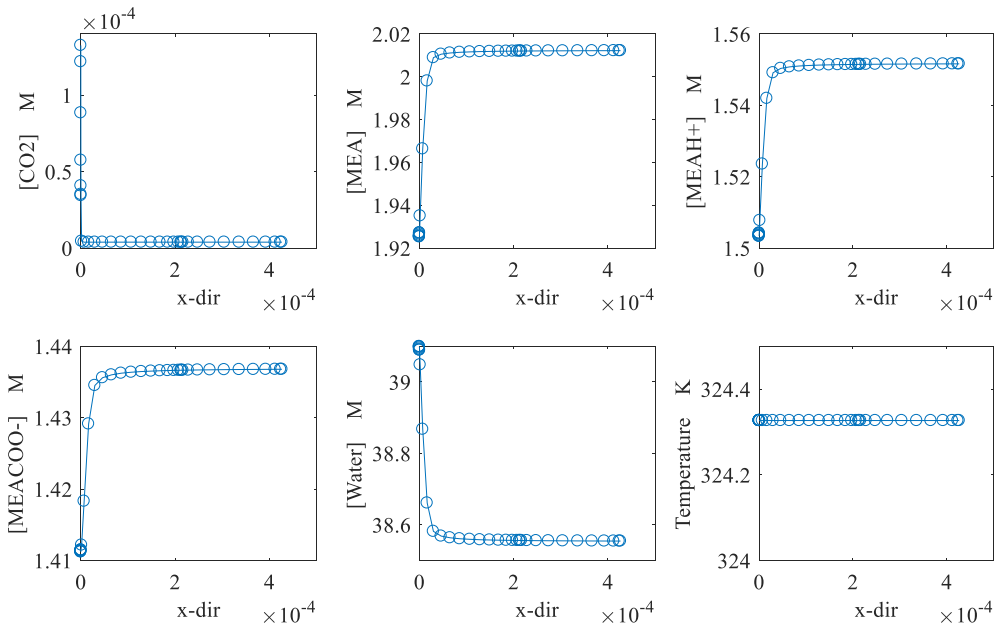


Fig.12 Concentration and temperature profiles in the liquid film at 0.1 sec for the NGCC case in the top section of the absorber.

The concentration and temperature profiles of different species in the liquid film are shown in fig. 12 at 0.1 sec of contact time. Concentrations of CO₂, free MEA, MEA⁺H, and MEACOO⁻ decrease close to the gas-liquid interface and H₂O concentration increases due to condensation at 0.1 sec. In case C4, even though the temperature difference between gas and liquid is very small, still the heat transfer effects are high due to condensation of H₂O, but in this case also the reaction with CO₂ plays a role.

Cement plant case (case C5):

The heat and mass transfer effects in the absorber top section were studied for the cement plant case with conditions given in table 1 for case C5. The 3-D profiles for concentrations and temperature are given as shown in fig. 13.

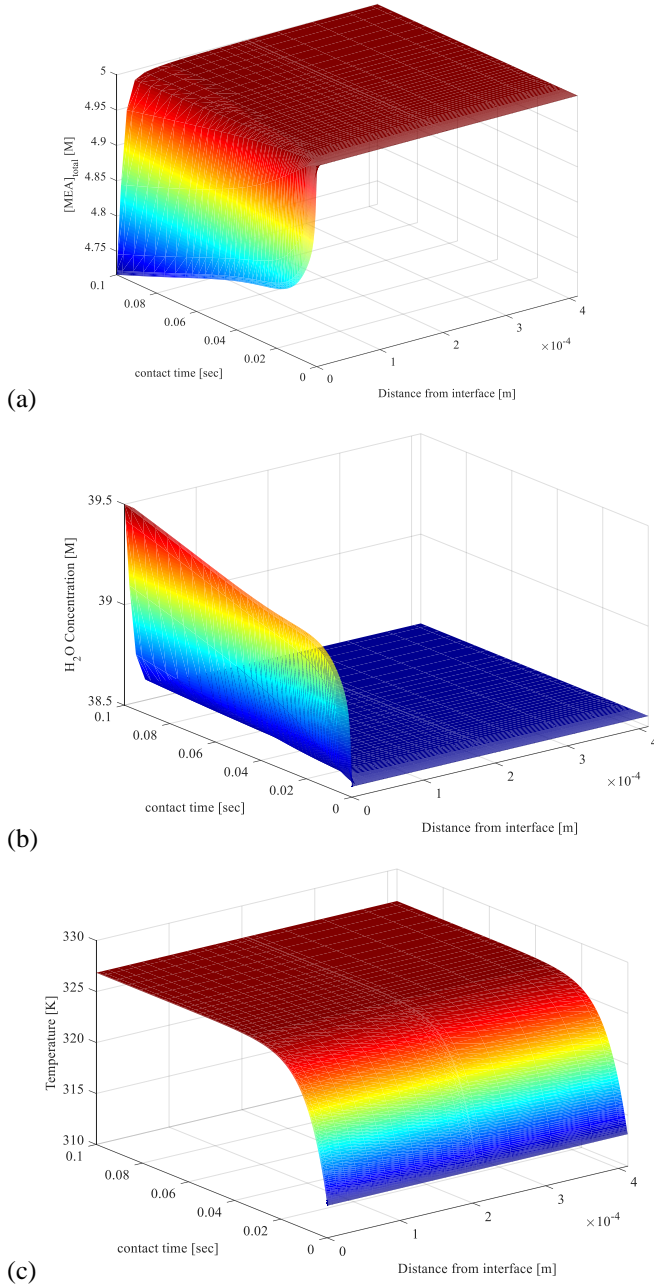


Fig.13 (a) Total MEA (b) H₂O and (c) temperature profiles in the liquid film for cement plant case C5 in the top section of the absorber

Interface profiles for temperature and water concentration and heat transfer contributions are shown in fig. 14. In the top section of the absorber, the temperature profile is opposite to the profile shown for case C3 at the bottom. The liquid temperature increases due to condensation of water and therefore water concentration increases and total MEA concentration decreases with time. It is

observed that at the absorber top for cement plant case (case C5), only condensation of water occurs. The rate of water condensation is high at the starting of gas-liquid contact and the temperature of the liquid increases rapidly up to 0.02 sec. The effect of concentration and temperature due to condensation on reaction rates ratio, is clearly seen in fig. (d) and (e) given in Appendix B. The reaction rates have opposite trends in absorber top section compared to the trends in absorber bottom section i.e., the ratio decreases in the starting of the gas-liquid contact and then becomes almost constant after 0.04 sec. It is also observed that reaction rate given by $r_{CO_2-H_2O}$ is higher compared to r_{CO_2-MEA} .

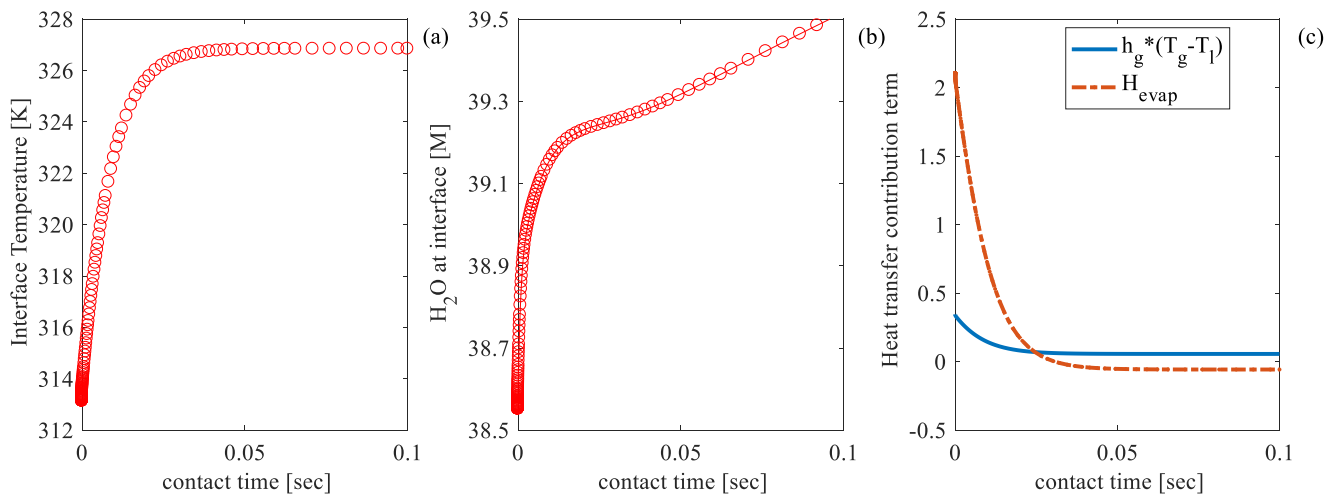
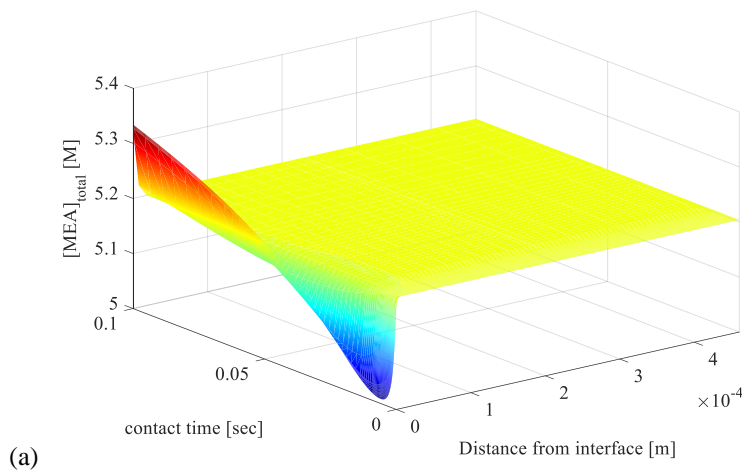


Fig.14 (a) Temperature, (b) H₂O concentration profiles and (c) Heat transfer contributions with respect to time at the interface cement plant case C5 in the top section of the absorber.

Absorber bottom pinch (C6):

In the last case the gas and liquid temperatures are equal. The conditions are given in the table 1. The gas is considered to be over-saturated at the given liquid temperature and composition. The temperature, total MEA and water concentration profiles are given in fig. 15.



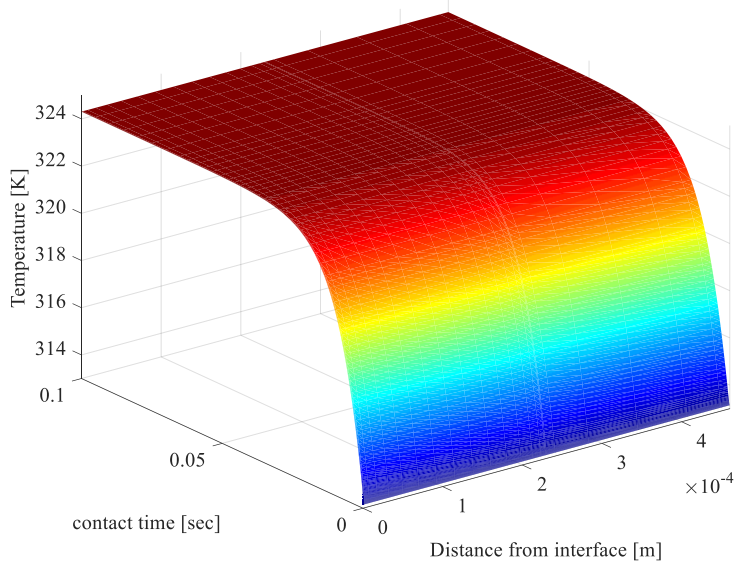
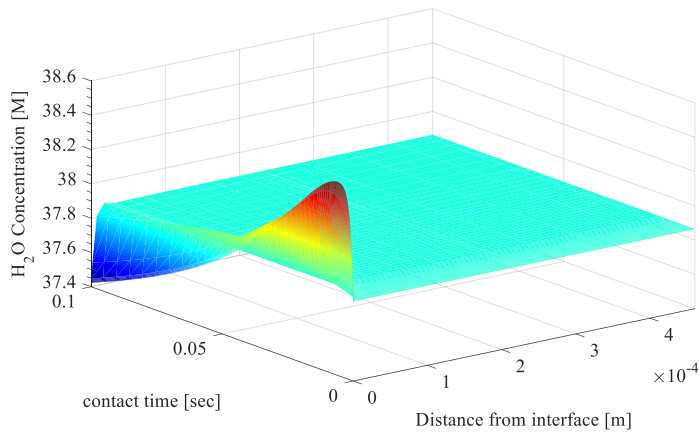


Fig.15 (a) Total MEA (b) H₂O and (c) temperature profiles in the liquid film for case C6

It is seen that first condensation of water occurs and the liquid temperature increases above the gas temperature and then evaporation starts. Total MEA, H₂O and temperature profiles show the same trends as seen in case C2. Due to the liquid temperature rise, the equilibrium at the gas –liquid interface changes and the equilibrium CO₂ pressure becomes higher than the CO₂ partial pressure in the gas phase. As the CO₂ driving force direction changes, CO₂ desorption takes place.

Interface temperature, H₂O and sensible and latent heat contribution profiles with respect to time are shown in fig. 16. As seen from fig. 16, condensation and liquid temperature increases rapidly. The temperature becomes constant as the convective heat transfer and latent heat transfer become equal but opposite in direction.

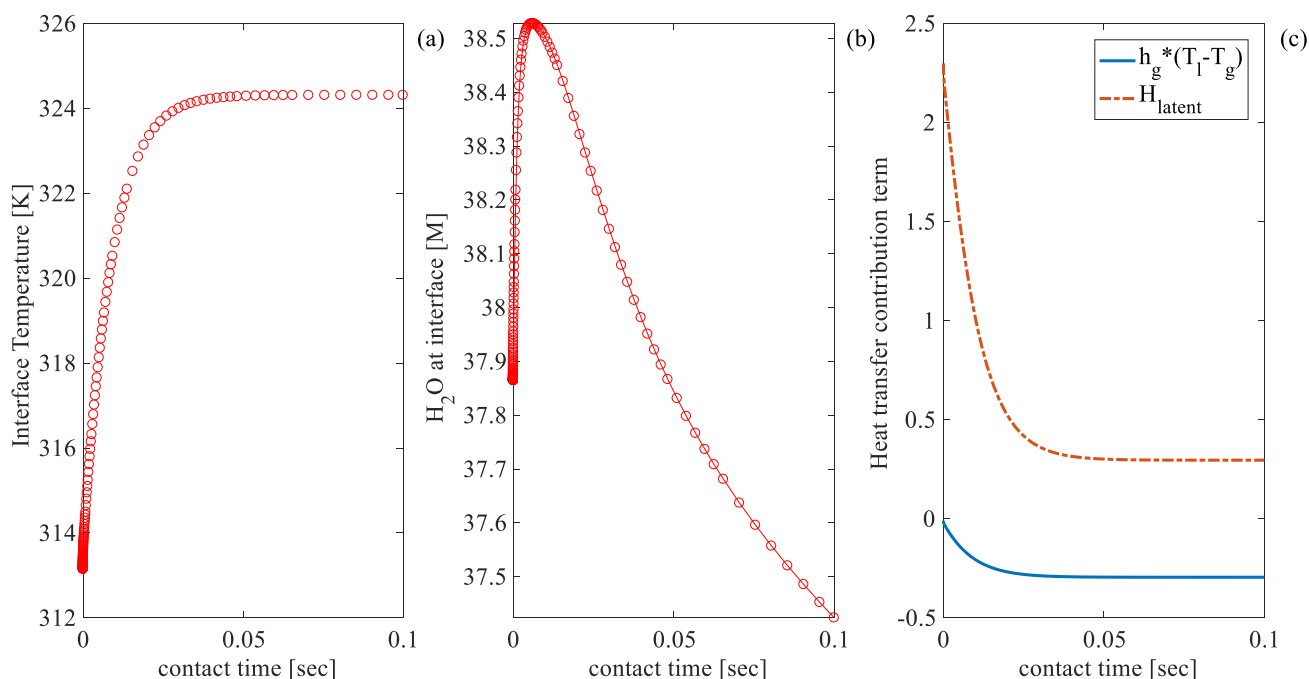


Fig.16 (a) Temperature, (b) H₂O concentration profiles and (c) Heat transfer contributions with respect to time at the interface for case C6

In case C6, initially absorption of CO₂ occurs and leads to desorption of CO₂ in the absorber bottom, which again reverts to absorption further up.

The effect of condensation and evaporation

In the previous sections we have seen that the time scales for thermal and component transport in the liquid phase are widely different. Heat is transferred very fast, giving practically flat temperature profiles in the liquid, whereas the transferring components create steep gradients close to the interface making the interface concentrations change rapidly. This can have an effect on the CO₂ mass transfer rate. In order to evaluate the studied effects of inclusion of evaporation and condensation phenomena on the CO₂ mass transfer rates, the CO₂ transfer, over the first 0.1 sec., for all cases was calculated and compared with cases without the inclusion of evaporation and condensation. For the industrial cases, it was seen that the change (decrease) in the CO₂ mass transfer flux is highest for case C1 and the change is about 5%, which is a significant decrease. The change in CO₂ flux is less than 1% for the four other industrial cases. In case 6, a situation resembling an absorber bottom pinch, was simulated. In this case the CO₂ flux sign changes and desorption occurred when taking the evaporation and condensation effects into account, whereas, without these effects, absorption was predicted. Also, the individual case fluxes after 0.05 sec. were compared and here we see that the largest effects were found when the driving forces and initial fluxes were large. In Case

3, with large initial flux, the flux without taking evaporation and condensation into account was only half the flux with these effects accounted for. In the other cases the differences were smaller.

Thus, there is change in reaction rates due to evaporation and condensation of water in the absorber column both at the bottom and top sections. The change in mass transfer rates gives rise to steep and rapidly changing interfacial concentration gradients. For most of the industrial cases these gradients did not significantly affect the absorption rate of CO₂. However, for the extreme case of warm unsaturated exhaust from an NG fired plant, case 1, and for the near pinch situation, case 6, significant changes to the CO₂ absorption rates were found.

Both CO₂ latent heat and MEA evaporation latent heat are small compared to the latent heat transfer due to evaporation of water. MEA evaporation counts for less than 1% of the total latent heat transfer and CO₂ latent heat due to transfer from gas to liquid is less than 5% (maximum 5% in case C2) of the total latent heat transfer. Also the heat of absorption is found to play a small role in the initial temperature change. It is basically the water evaporation and condensation that dominates.

In the present study, the effect of convective flux in the gas phase due to evaporation and condensation was not considered and will be studied in future work and it is believed that taking this into account may have a larger influence on the CO₂ fluxes than the concentration effects studied in the present paper.

5 Conclusions

A combined heat and mass transfer model has been developed in this work. The effect of transfer of components (MEA, H₂O, CO₂) from one phase to another (gas to liquid and vice versa) on the concentrations of species in the liquid phase was included in the model. Six different cases were considered to understand the degree of impact on heat and mass transfer by condensation and evaporation of H₂O. The model predictions gave reasonable profiles for both condensation and evaporation cases. Significant temperature effects were seen both in water evaporation and condensation cases at the bottom and top sections of the absorber column. It was seen that the liquid temperature rise depends on the water saturation level in the gas phase at the given liquid temperature and the difference between gas and liquid temperatures. The reaction rates vary due to both evaporation and condensation of water. The temperature change due to evaporation or condensation of water happens very rapidly. In some cases, it is seen that initially the process starts with evaporation of water and switches to condensation due to temperature drop below the saturation temperature and vice versa. In the case simulating absorber pinch, it was seen that initially the process starts with absorption of CO₂ but rapidly shifts to desorption of CO₂ as the driving force decreases due to liquid

temperature rise above the gas temperature when condensation and evaporation of water was taken into account. The temperature profiles are uniform throughout the liquid film at a given time but concentration gradients are seen close to the gas-liquid interface for all cases. From the detailed temperature, concentrations and reaction rates profiles, it is found that solution of the model equations is only required up to 10 μm distance from the interface (approximately 3% of liquid film thickness). This information can be used in the full-scale CO₂ absorption process simulators so that the interface transfer models can incorporate the heat-transfer effects in addition to the mass transfer and chemical reactions. Although the effect of evaporation and condensation was seen to have significant effect on interface concentrations and temperatures, changes in the CO₂ flux were found to be small for most cases. However, a 5% change was seen for NGCC case and for the near pinch conditions, a reversion of the CO₂ transfer was found.

ACKNOWLEDGEMENT:

Financial support from the Faculty of Natural Sciences at the Norwegian University of Science and Technology is greatly acknowledged.

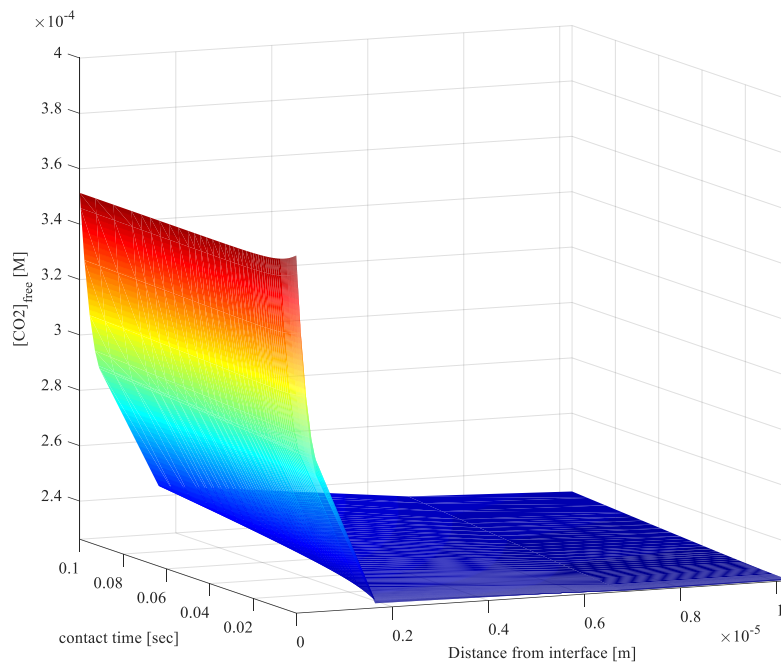
The authors also thank Diego Pinto for reviewing and commenting the manuscript.

References

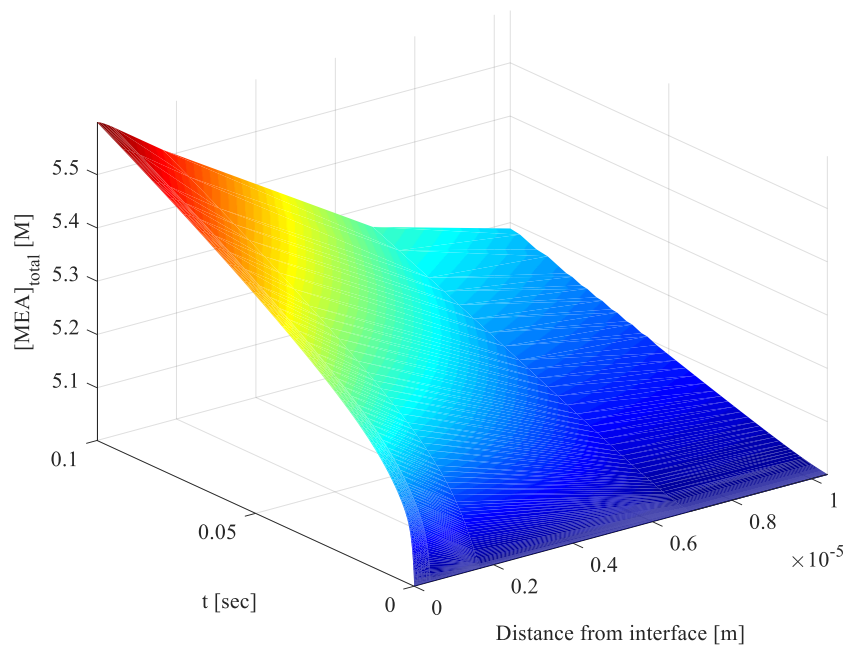
- Arora, S., Dhaliwal, S.S., Kukreja, V.K., 2006a. Simulation of washing of packed bed of porous particles by orthogonal collocation on finite elements. *Comput. Chem. Eng.* 30, 1054–1060. doi:10.1016/j.compchemeng.2006.02.002
- Arora, S., Dhaliwal, S.S., Kukreja, V.K., 2006b. Application of orthogonal collocation on finite elements for solving non-linear boundary value problems. *Appl. Math. Comput.* 180, 516–523. doi:10.1016/j.amc.2005.12.036
- Carey, G.F., Finlayson, B.A., 1975. Orthogonal collocation on finite elements. *Chem. Eng. Sci.* 30, 587–596. doi:10.1016/0009-2509(75)80031-5
- Cheng, S., Meisen, A., Chakma, A., 1996. Predict Amine Solution Properties Accurately. *Hydrocarb. Process.* 75.
- Chow, L.C., Chung, J.N., 1983. Evaporation of water into a laminar stream of air and superheated steam. *Int. J. Heat Mass Transf.* 26, 373–380. doi:10.1016/0017-9310(83)90041-8
- Duarte, B.P.M., Portugal, A.A.T.G., 1995. Moving finite elements method applied to the solution of front reaction models: causticizing reaction. *Comput. Chem. Eng., European Symposium on Computer Aided Process Engineering* 3-5 19, Supplement 1, 421–426. doi:10.1016/0098-1354(95)87073-3
- Geankoplis, C., 2003. *Transport Processes and Separation Process Principles*, 4th ed. ed. Prentice-Hall.
- Ghanaei, E., Rahimpour, M.R., 2010. Evaluation of orthogonal collocation and orthogonal collocation on finite element method using genetic algorithm in the pressure profile prediction in petroleum reservoirs. *J. Pet. Sci. Eng.* 74, 41–50. doi:10.1016/j.petrol.2010.08.005
- Hartono, A., Mba, E.O., Svendsen, H.F., 2014. Physical Properties of Partially CO₂ Loaded Aqueous Monoethanolamine (MEA). *J. Chem. Eng. Data* 59, 1808–1816. doi:10.1021/je401081e
- Hassan, S.M.N., 2005. Techno-economic study of CO₂ capture process for cement plants (Master Thesis). University of Waterloo, Ontario, Canada.
- Kale, C., Górak, A., Schoenmakers, H., 2013. Modelling of the reactive absorption of CO₂ using mono-ethanolamine. *Int. J. Greenh. Gas Control* 17, 294–308. doi:10.1016/j.ijggc.2013.05.019
- Ko, J.-J., Tsai, T.-C., Lin, C.-Y., Wang, H.-M., Li, M.-H., 2000. Diffusivity of Nitrous Oxide in Aqueous Alkanolamine Solutions. *J. Chem. Eng. Data* 46, 160–165. doi:10.1021/je000138x
- Kohl, A.L., Nielsen, R., 1997. *Gas purification*, 5th ed. ed. Gulf Pub, Houston, Tex.
- Kvamsdal, H.M., Hillestad, M., 2012. Selection of model parameter correlations in a rate-based CO₂ absorber model aimed for process simulation. *Int. J. Greenh. Gas Control* 11, 11–20. doi:10.1016/j.ijggc.2012.07.013
- Kvamsdal, H.M., Rochelle, G.T., 2008. Effects of the Temperature Bulge in CO₂ Absorption from Flue Gas by Aqueous Monoethanolamine. *Ind. Eng. Chem. Res.* 47, 867–875. doi:10.1021/ie061651s
- Liang, Z., Fu, K., Idem, R., Tontiwachwuthikul, P., 2016. Review on current advances, future challenges and consideration issues for post-combustion CO₂ capture using amine-based absorbents. *Chin. J. Chem. Eng.* 24, 278–288. doi:10.1016/j.cjche.2015.06.013
- Liang, Z. (Henry), Rongwong, W., Liu, H., Fu, K., Gao, H., Cao, F., Zhang, R., Sema, T., Henni, A., Sumon, K., Nath, D., Gelowitz, D., Srisang, W., Saiwan, C., Benamor, A., Al-Marri, M., Shi, H., Supap, T., Chan, C., Zhou, Q., Abu-Zahra, M., Wilson, M., Olson, W., Idem, R., Tontiwachwuthikul, P. (PT), 2015. Recent progress and new developments in post-combustion carbon-capture technology with amine based solvents. *Int. J. Greenh. Gas Control*, Special Issue commemorating the 10th year anniversary of the publication of the

- Intergovernmental Panel on Climate Change Special Report on CO₂ Capture and Storage 40, 26–54. doi:10.1016/j.ijggc.2015.06.017
- Luo, X., Knudsen, J.N., de Montigny, D., Sanpasertparnich, T., Idem, R., Gelowitz, D., Notz, R., Hoch, S., Hasse, H., Lemaire, E., Alix, P., Tobiesen, F.A., Juliussen, O., Köpcke, M., Svendsen, H.F., 2009. Comparison and validation of simulation codes against sixteen sets of data from four different pilot plants. *Energy Procedia, Greenhouse Gas Control Technologies 9 Proceedings of the 9th International Conference on Greenhouse Gas Control Technologies (GHGT-9)*, 16–20 November 2008, Washington DC, USA 1, 1249–1256. doi:10.1016/j.egypro.2009.01.164
- Neveux, T., Le Moullec, Y., Corriou, J.-P., Favre, E., 2013. Modeling CO₂ Capture in Amine Solvents: Prediction of Performance and Insights on Limiting Phenomena. *Ind. Eng. Chem. Res.* 52, 4266–4279. doi:10.1021/ie302768s
- Putta, K.R., Pinto, D.D.D., Svendsen, H.F., Knuutila, H.K., 2016. CO₂ absorption into loaded aqueous MEA solutions: Kinetics assessment using penetration theory. *Int. J. Greenh. Gas Control* 53, 338–353. doi:10.1016/j.ijggc.2016.08.009
- Puxty, G., Rowland, R., Attalla, M., 2010. Comparison of the rate of CO₂ absorption into aqueous ammonia and monoethanolamine. *Chem. Eng. Sci.* 65, 915–922. doi:10.1016/j.ces.2009.09.042
- Ralph H. Weiland, Nathan A. Hatcher, 2011. Stable operating limits for amine absorbers. *Contactors* 5.
- Razi, N., Svendsen, H.F., Bolland, O., 2014. Assessment of mass transfer correlations in rate-based modeling of a large-scale CO₂ capture with MEA. *Int. J. Greenh. Gas Control* 26, 93–108. doi:10.1016/j.ijggc.2014.04.019
- Razi, N., Svendsen, H.F., Bolland, O., 2013a. Validation of mass transfer correlations for CO₂ absorption with MEA using pilot data. *Int. J. Greenh. Gas Control* 19, 478–491. doi:10.1016/j.ijggc.2013.10.006
- Razi, N., Svendsen, H.F., Bolland, O., 2013b. The Impact of Design Correlations on Rate-based Modeling of a Large Scale CO₂ Capture with MEA. *Energy Procedia, GHGT-11* 37, 1977–1986. doi:10.1016/j.egypro.2013.06.078
- Reid, Prausnitz, J. M., Poling, B. E., 1986. *The Properties of Gases and Liquids*. McGraw-Hill, New York.
- Rochelle, G.T., 2009. Amine Scrubbing for CO₂ Capture. *Science* 325, 1652–1654. doi:10.1126/science.1176731
- Seaward, D.O., Segall, B.A., Ott, C.R., Donatelli, A.A., 1984. The Effects of Evaporation and Condensation on an Absorption Process, in: Brutsaert, W., Jirka, G.H. (Eds.), *Gas Transfer at Water Surfaces*, Water Science and Technology Library. Springer Netherlands, pp. 57–64. doi:10.1007/978-94-017-1660-4_6
- Snijder, E.D., te Riele, M.J.M., Versteeg, G.F., van Swaaij, W.P.M., 1993. Diffusion coefficients of several aqueous alkanolamine solutions. *J. Chem. Eng. Data* 38, 475–480. doi:10.1021/je00011a037
- Tobiesen, F.A., Juliussen, O., Svendsen, H.F., 2008. Experimental validation of a rigorous desorber model for post-combustion capture. *Chem. Eng. Sci.* 63, 2641–2656. doi:10.1016/j.ces.2008.02.011
- Tobiesen, F.A., Svendsen, H.F., Juliussen, O., 2007. Experimental validation of a rigorous absorber model for CO₂ postcombustion capture. *AIChE J.* 53, 846–865. doi:10.1002/aic.11133
- Versteeg, G.F., Van Swaaij, W., 1988. Solubility and diffusivity of acid gases (carbon dioxide, nitrous oxide) in aqueous alkanolamine solutions. *J. Chem. Eng. Data* 33, 29–34. doi:10.1021/je00051a011
- Wang, M., Lawal, A., Stephenson, P., Sidders, J., Ramshaw, C., 2011. Post-combustion CO₂ capture with chemical absorption: A state-of-the-art review. *Chem. Eng. Res. Des., Special Issue on Carbon Capture & Storage* 89, 1609–1624. doi:10.1016/j.cherd.2010.11.005

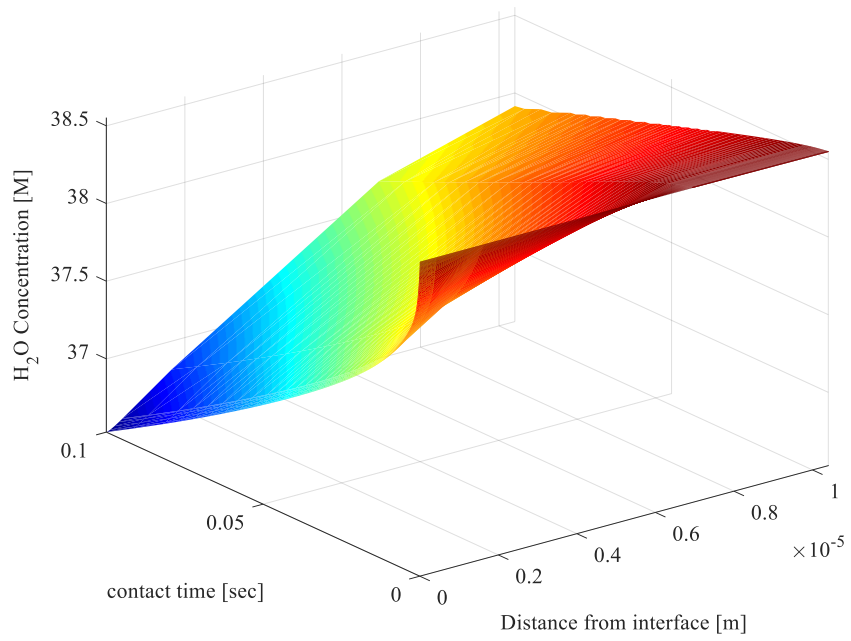
Appendix A1 (NGCC case)



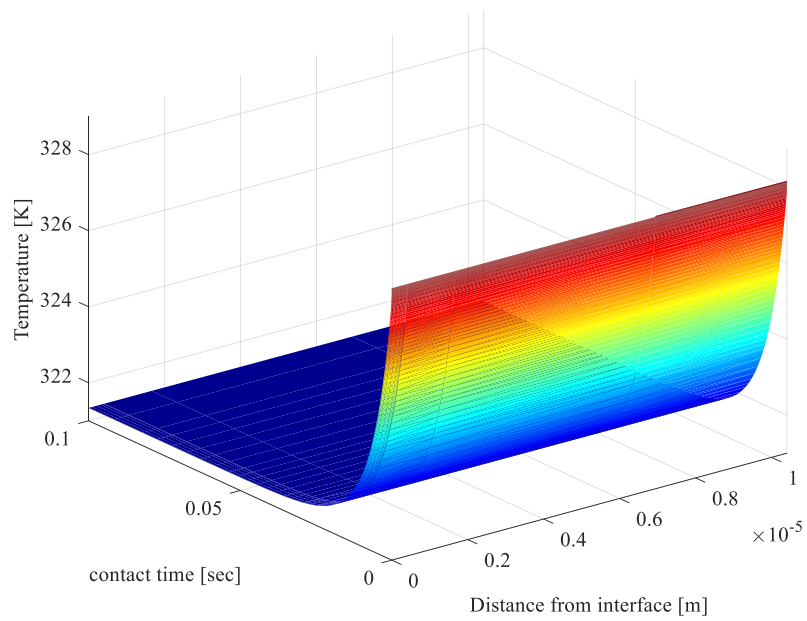
(i) Zoomed total MEA profiles from case C1



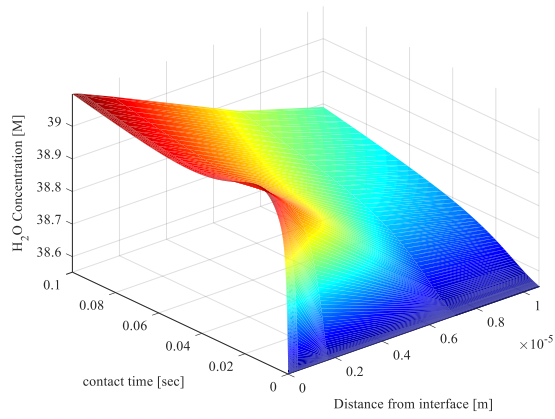
(ii) Zoomed total MEA profiles from case C1



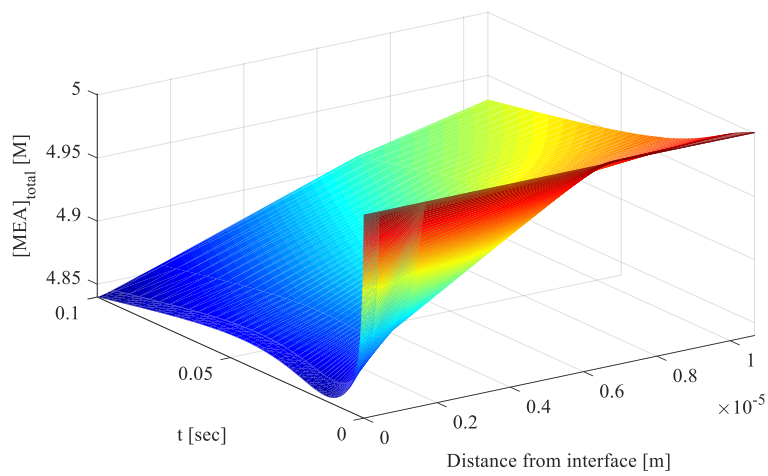
(iii) Zoomed H₂O profiles from case C1



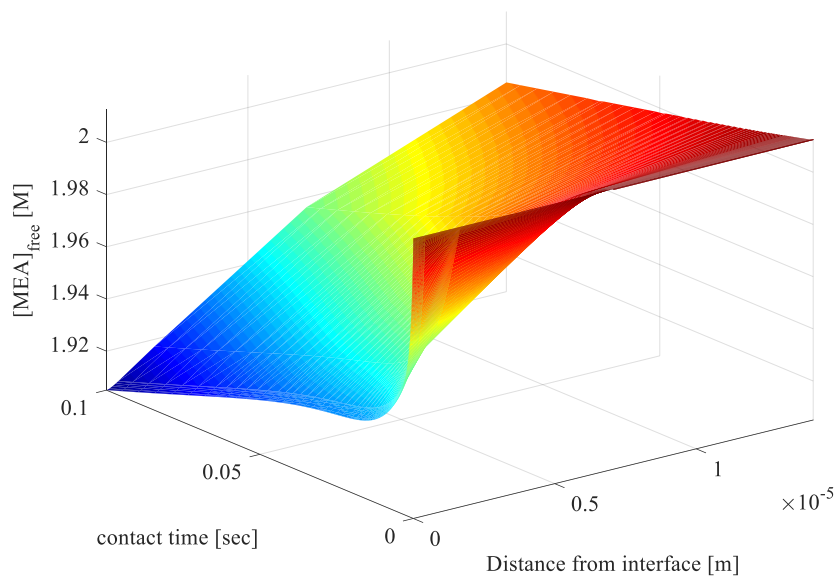
(iv) Zoomed temperature profiles for case C1



(v) Zoomed H₂O profiles from case C4



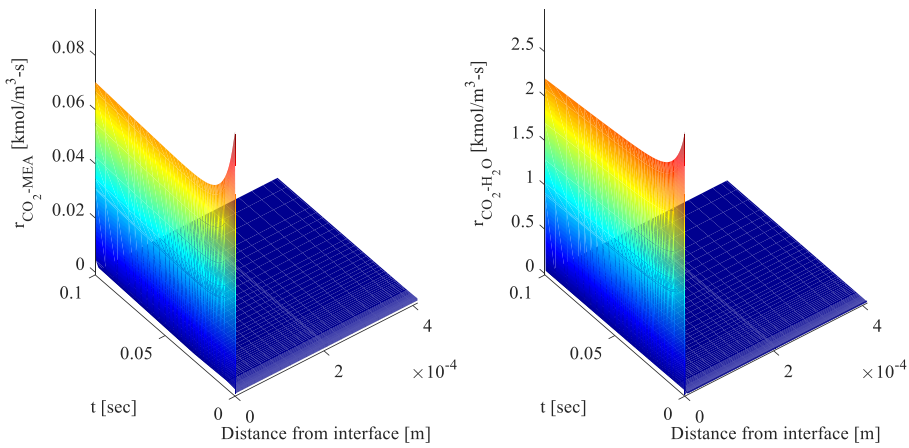
(vi) Zoomed total MEA profiles from case C4



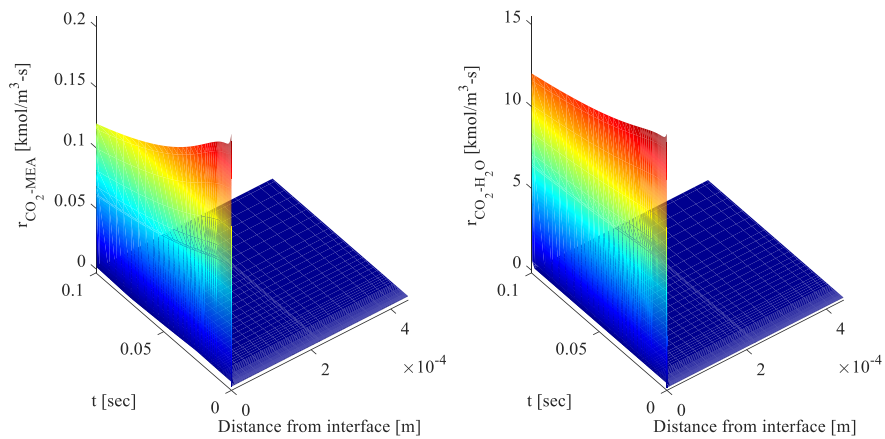
(vii) Zoomed free MEA profiles from case C4

Appendix B

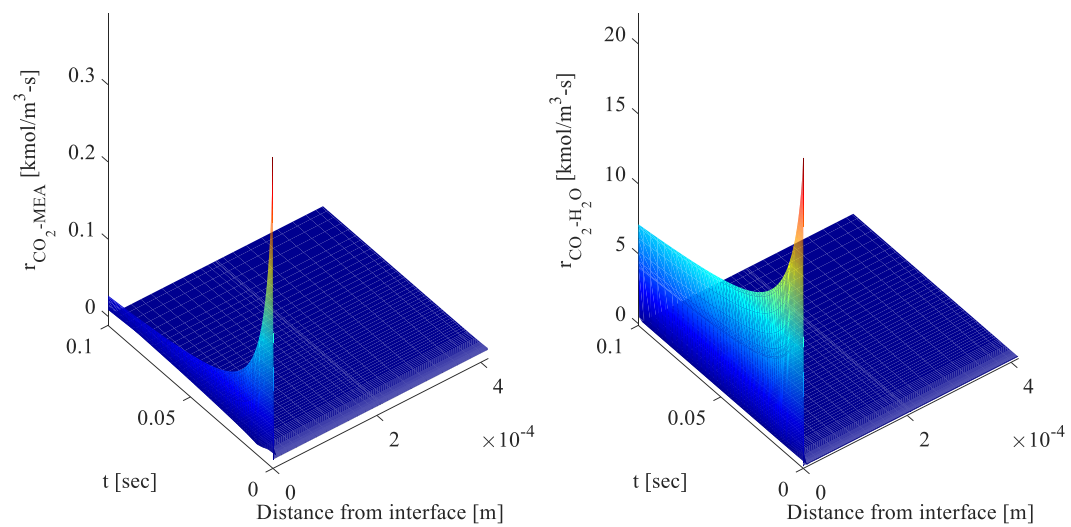
At the absorber bottom: reaction rates profiles



(a) Case C1: NGCC case

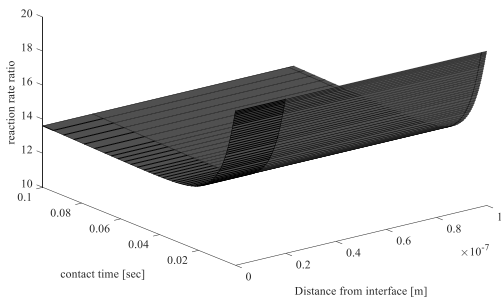
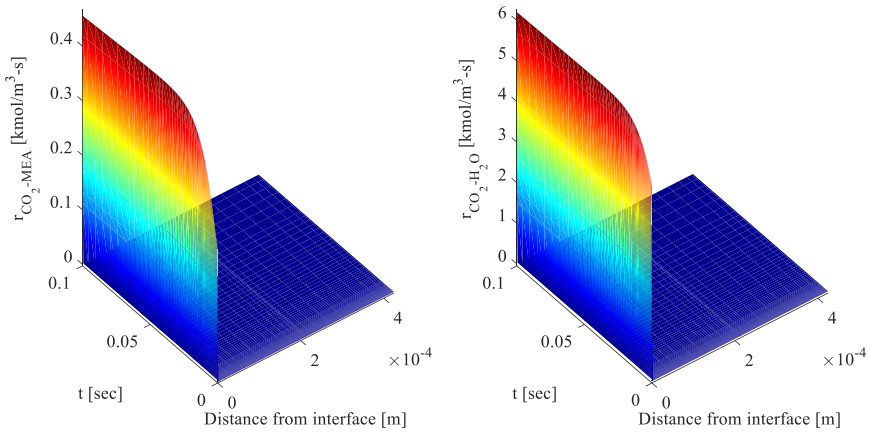


(b) Case C2: Coal-fired power plant case

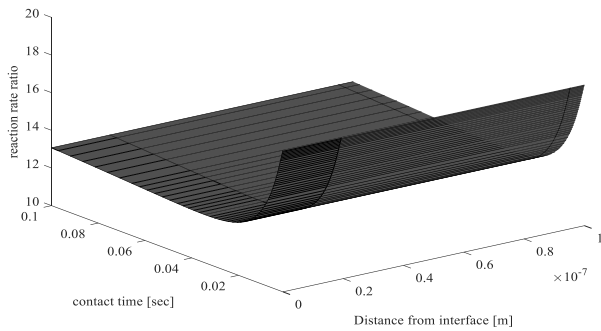
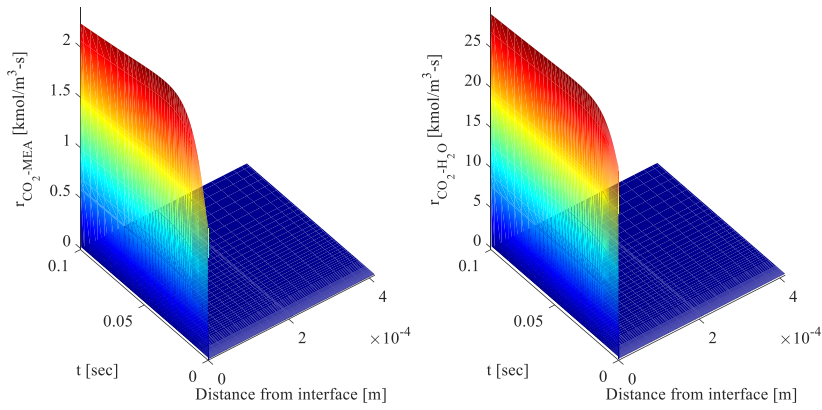


(c) Case C3: Cement plant case

In the absorber top: reaction rates profiles



(d) Case C4: NGCC case



(e) Case C5: Cement plant case